



UPPSALA
UNIVERSITET

UPTEC ES 20020

Examensarbete 30 hp
Juni 2020

A Comparison of Grid-Forming and Grid-Following Control of VSCs

Pontus Roos



UPPSALA
UNIVERSITET

Teknisk- naturvetenskaplig fakultet
UTH-enheten

Besöksadress:
Ångströmlaboratoriet
Lägerhyddsvägen 1
Hus 4, Plan 0

Postadress:
Box 536
751 21 Uppsala

Telefon:
018 – 471 30 03

Telefax:
018 – 471 30 00

Hemsida:
<http://www.teknat.uu.se/student>

Abstract

A Comparison of Grid-Forming and Grid-Following Control of VSCs

Pontus Roos

Variable renewable energy sources are today increasingly integrated in the power system as a step towards the renewable society. The large-scale introduction of converter-based energy sources brings challenges in terms of reduced damping to the power system due to the reduced number of synchronous generators. This can be manifested as high rate-of-change-of-frequency and decreased grid stability. To forestall this reduced performance, it is suggested that the grid-following control of today's converters are restructured to a grid-forming control, enabling the converter to behave closer to a synchronous machine.

This thesis compares grid-following and grid-forming control and seeks to further describe this grid-forming behavior by applying a grid-forming control method on an energy storage enhanced STATCOM-system. A continuous time model and a linearized model based on state space representations are constructed in order to investigate the grid-forming behavior but also how the converter stability is affected by a restructure from grid-following to grid-forming control.

The results indicate that the investigated grid-forming control method displays a behavior similar to synchronous machines and incorporates the ability to provide frequency response services and so called "synthetic inertia" to the grid. The results also show that the stability of the converter (the ability to provide a bounded output when the system is perturbed) is ensured when the control method is restructured from grid-following to grid-forming and that the investigated grid-forming method is stable also in weak grid situations.

Handledare: Theodore Soong
Ämnesgranskare: Urban Lundin
Examinator: Petra Jönsson
ISSN: 1650-8300, UPTEC ES 20020

Populärvetenskaplig sammanfattning

Förnybara energikällor integreras idag i en allt snabbare takt i elkraftsystemet, både i Sverige och internationellt. Dessa energikällor är ofta variabla i sin elproduktion då de är beroende av okontrollerbara källor som vindens hastighet, eller solens instrålning. Det medför att dessa energikällor uppvisar ett annorlunda beteende jämfört med kontrollerbara energikällor som t.ex. vattenkraft och kärnkraft.

Vatten- och kärnkraftverk använder så kallade synkrona generatorer för att generera elektricitet. Att generatorn är synkron innebär att den roterar med samma elektriska frekvens som den elektriska nät-frekvensen (som i Sverige är 50 Hz) och generatoren är direkt kopplad till elnätet. Det innebär att samtliga synkrona generatorer i elkraftsystemet roterar med samma frekvens och tillsammans bidrar till att hålla frekvensen konstant. Vid alla tidpunkter måste det råda balans mellan elproduktion och elkonsumption i systemet. Om så inte sker kommer frekvensen avvika från sitt nominella värde, något som kan få mycket allvarliga konsekvenser, till exempel större strömbrott under en längre tid. Fördelell med synkrongeneratorer är att de försöker hjälpas åt att bibehålla nätfrekvensen på 50 Hz. Om frekvensen på elnätet sjunker så känner synkrongeneratorn av det och energi från generatorns roterande massa (så kallad svängmassa) levereras till elnätet för att motverka den sjunkande frekvensen. Denna förenklade beskrivning illustrerar hur synkrongeneratorer bidrar till att upprätthålla frekvensen på 50 Hz. Synkrongeneratorer bidrar även med att upprätthålla spänningsnivån på elnätet.

De variabla förnybara källorna ansluts ofta via kraftelektronik för att leverera den producerade effekten till elnätet. Det innebär att dessa energikällor inte kan bidra med samma systemtjänster i form av naturlig svängmassa och spänningsstabilitet. Då andelen variabla energikällor som är anslutna till elnätet ökar kommer andelen synkrongeneratorer att minska och därav elnätets förmåga att motstå frekvensändringar som i sin tur medför en försämrad systemstabilitet.

Denna studie syftar till att identifiera nya kontrollmetoder, så kallad grid-forming control (eng.) eller nätformande kontroll, för kraftomvandlare som möjliggör så att dessa kan bidra med samma stödtjänster som synkrongeneratorer och därmed möjliggöra en ökad integration av variabel, förnybar energi. I studien modelleras en kraftomvandlare, ett STATCOM (static synchronous compensator) -system, kompletterat med ett energilager. Genom simuleringar undersöks skillnaderna mellan en nätföljande kontrollmetod och den föreslagna nätformande kontrollmetoden. Det undersöks även om den nya kontrollmetoden möjliggör ett beteende som efterliknar det hos synkrongeneratorer. Slutligen undersöks om kraftomvandlarens stabilitet påverkas av bytet av kontrollmetod.

Dagens kraftelektroniksystem använder främst en så kallad nätföljande kontrollmetod. Det innebär att kraftelektroniksystems utsignaler (ström och spänning) anpassas efter den rådande nätsituationen. En nätföljande enhet kommer därav att bete sig som en strömkälla. Ett nätformande system kommer istället att arbeta kring en definierad arbetspunkt och anpassa utsignalerna därefter. Den kommer därmed istället bete sig som en spänningsskälla.

TVÅ olika simuleringsmodeller utvecklades i arbetet för att undersöka prestandan hos en nätformande kontrollmetod. En tidskontinuerlig modell implementerades i Simulink och en linjäriserad modell av tillståndsbeskrivningar upprättades av STATCOM-systemet. Dessa två modeller validerades därefter mot varandra för att säkerställa att de beskriver samma dynamik. Den tidskontinuerliga modellen användes för att simulaera systemsvar i olika situationer och den linjäriserade modellen för att undersöka stabilitetsaspekter.

Genom att simulaera en förändring av nätfrekvensen kan det studeras hur den nätformande kontrollme-

toden reglerar den utlevererande aktiva effekten. Resultaten visar att enheten, likt en synkrongenerator, sänder ut en ökad effekt då frekvensen sjunker och en minskad effekt då frekvensen överskrider 50 Hz. Detta innebär att förändringen av kontrollmetoden har möjliggjort för enheten att vara med och svara upp mot frekvensförändringar och den uppvisar en form av syntetisk svängmassa.

En ingående analys av hur kraftomvandlarens stabilitet påverkas av förändringen från en nätföljande till nätförmande kontrollmetod utförs i studien. Även de olika parametrarna i den nätförmande kontrollmetoden undersöks ingående. Analysen visar att enheten fortfarande uppvisar ett stabilt beteende med den nätförmande kontrollmetoden och att metoden introducerar en flexibilitet som gör det möjligt att anpassa kontrollmetoden till olika nätsituationer.

I studien rekommenderas att fortsatta studier utförs på den nätförmade kontrollmetoden, bland annat med avseende på de begränsningar energilagret medför och de likheter som den nätföljande och nätförmande kontrollmetoden uppvisar.

Executive Summary

The penetration levels of converter-based energy sources continue to increase, introducing the possibility of a 100 % converter-based transmission system in the future [1], [2]. The market demand for converters with grid-forming control will be heavily increased in such a future. It is therefore beneficial to have good insights on the grid-forming behavior and to be able to offer such solutions to the market.

This thesis introduces three different grid-forming control methods and further analyzes one of these methods. The results indicate that the investigated grid-forming control method shows a behavior similar to that of synchronous generators since the converter is able to operate around a specific operating point and adjust its output accordingly. The investigation also shows that the control method has the ability to provide frequency response services and so called “synthetic inertia” to the grid. The results also indicate that the stability of the converter is ensured when the control is restructured from a grid-following to a grid-forming control. Meaning that the converter is able to provide a bounded output when the system is perturbed.

It is suggested that the research on grid-forming control is to be continued and the origin of the similarities of a grid-following and grid-forming synchronization is further investigated. An investigation of the two methods that were not further analyzed in this study is also recommended. Future studies should also investigate how the limitations set by the energy storage system can influence the grid-forming behavior and consider the fault ride thorough capability and the ability to limit the converter inrush current.

Acknowledgement

This project has been performed for ABB Power Grids but also marks my completion of the Master of Science program in Energy Systems Engineering at Uppsala University and the Swedish University of Agricultural Sciences.

I would like to take the opportunity to express my gratitude to those who have made this project possible. The help and continued support from my supervisor, Theodore Soong, has been essential for the completion of this project. Thank you, Theo, for all your advice and encouragement throughout this project and for answering my many questions.

Many thanks to David Strinnholm for your interest and continued support during the project. I would also like to thank my subject reviewer, Urban Lundin at Uppsala University, for your guidance and feedback on the report.

Lastly, I would like to thank ABB Power Grids and its personnel for welcoming me to the organization and providing me with the chance to perform this project.

Thank you all!

Pontus Roos
Uppsala, June 2020

Contents

1	Introduction	1
1.1	Task definition	2
1.1.1	Delimitations	2
1.2	Disposition of the Report	2
2	Background	3
2.1	FACTS-devices	3
2.2	Transfer Functions, System Response & State Space Models	4
2.2.1	State Space Representation	6
2.3	Reference Frames used in the Control of VSCs	7
2.3.1	The $\alpha\beta$ -frame	7
2.3.2	The dq-frame	8
3	VSC Control Modes	10
3.1	Grid-Following Control	10
3.1.1	Grid-Following Synchronization	11
3.2	Grid-Forming Control	11
3.2.1	The Swing Equation and Power Transfer Equations	12
3.2.2	Frequency Behavior	14
3.2.3	Voltage Behavior	16
3.2.4	Summary and Discussion of Grid Forming Control Methods	20
4	Development of Simulation Models	22
4.1	Simulink Model	22
4.2	State Space Model	24
4.2.1	Creation of State Space Representation in the dq-frame	26
4.3	Model Validation	27
4.3.1	PLL-system	27
4.3.2	SPC-system	28
5	Simulation Results	30
5.1	Continuous Time Simulations	30
5.1.1	Frequency Behavior	30
5.1.2	Voltage Behavior	33
5.2	Stability Assessment and Identification of Poles	34
5.2.1	Influence of the Virtual Admittance	35
5.2.2	Participation Factors	36
5.2.3	Comparison of Pole Locations With a Grid Following PLL-System	40
5.2.4	Grid Strength Impact on Pole Locations	42
5.2.5	SPC Power Loop Parameters	45
6	Discussion	47
7	Conclusion	50

Bibliography	51
A Analysis of Pole Locations for Model Components	53
B Other Grid Forming Control Methods	57
C Continued Model Validation	58

Chapter 1

Introduction

Traditionally, the electric power system consists of centralized generating units that supplies power to the consumers via long transmission lines. Today, the power system is entering a new era where variable renewable energy sources such as solar photovoltaics (PV) and wind power systems are increasingly introduced in the power system due to environmental and economic reasons. Several countries such as Ireland, Germany and Denmark have high levels of variable renewable energy in their power systems with an annual penetrations of more than 20 % at a national level [3]. Other countries are expected to follow in this direction. Sweden is one of the countries that wants to be in the forefront of this transition and the Swedish government have declared a goal of a 100% renewable electricity production by 2040 [4].

PV-systems and the majority of wind power systems are connected to the grid by the use of power electronics. Therefore, they will behave differently than the large generators used in hydro and nuclear power that spins synchronously with the grid frequency. This transition from generation with synchronous generators to converter-based renewable energy-systems will lower the available inertia in the grid due to the transition from rotating electrical machines to power electronics. Transmission system operators (TSOs), responsible for maintaining the electric frequency in the grid, are especially concerned with this problem. A grid with low inertia will experience a high rate-of-change-of-frequency (ROCOF) that introduces the possibility of larger frequency deviations and decreased stability in the grid. These larger frequency deviations, if large enough, can cause synchronous generators to lose synchronism which can trigger other events such as voltage and power imbalances that in turn can result in a total collapse of the power system [3]. Denis et al and Markovic et al foretell that with the current trends of increasing integration of variable renewable energy systems to the power grid, a future with a 100 % converter-based transmission system is possible [1], [2].

It is therefore of utmost importance to identify methods of integrating large portions of renewable sources without causing stability problems in the power system. To this date, most converter-based systems operate on a grid-following principle where a phase locked loop (PLL) is used to align with the grid voltage at the point of common coupling (PCC) of the converter. Thus, it “follows” the measured voltage by aligning and using the measured voltage as reference. These converters are not expected to respond on grid frequency changes [5]. It is suggested that in order to avoid the problems associated with low inertia, the control of converters should be restructured from a grid-following to a grid-forming control that are able to provide damping to frequency changes and whose behavior is more similar to that of a synchronous machine. This is possible since grid forming systems creates its own internal voltage reference angle based on the output power of the converter [6].

Energy storage enhanced power converters are prime candidates to provide this fast frequency and synthetic inertia behavior. A static synchronous compensator (STATCOM) supplemented by energy storage is a device suggested to serve this purpose. STATCOMs are normally operated in a grid following way and are used to support grids that has problems with voltage regulation and poor power factor. To be able to also offer fast frequency and synthetic inertia services to these networks could further increase network performance of weak grids. In the future, it may also be necessary for STATCOMs

to operate closer to grid forming control since TSOs could regulate, via grid code specifications, that future power converters should operate with grid forming control in order to mitigate the problems with an increasing penetration of variable renewable energy sources. The expected future increased renewable energy penetration in the power system and the countermeasures of TSOs motivates an in-depth investigation on the performance of grid-forming control methods.

1.1 Task definition

The objective of this master's thesis is to investigate grid-forming control implemented on a STATCOM-system complemented with an energy storage. Grid-forming control can be implemented in several ways. This thesis seeks to provide insights to the principles of grid-forming control and identify suitable methods of achieving grid-forming control. One such control method will be further analyzed and focus is placed on identifying the differences between a grid-forming and a grid-following control method in terms of frequency and voltage behavior. The thesis also seeks to investigate how the stability of the converter is affected when the control system is restructured from a grid-following to grid-forming.

The aforementioned objectives can be summarized into the following questions that the thesis seeks to answer:

- What is grid forming control and what does it mean to operate a converter with grid forming control in terms of frequency and voltage behavior?
- Can a STATCOM-system, complemented by energy storage, using grid forming control be used for fast frequency response services and provide synthetic inertia to the grid?
- How is the stability of the converter affected when the synchronization is restructured from grid-following to grid-forming?
- How is the converter stability affected in weak grid situations using grid-forming control?

1.1.1 Delimitations

Some simplifications and assumptions have been made in this thesis. The work is limited to only consider the case where no restrictions are placed on the energy storage system. The DC-side of the converter will therefore be modelled as a DC-voltage source. The thesis will identify and describe several grid-forming control methods, but the simulation work will be limited to one of these methods. The thesis also aims to investigate the performance in weak grid situations. In this study the weak grid investigation will be limited to consider a weak grid in terms of poor grid strength (in terms of voltage stability) but with high inertia. The converter is modelled in Simulink as an average-value voltage source converter and therefore disregard any detailed representation of the converter. Other assumptions regarding the simulation models are further described in Chapter 4.

1.2 Disposition of the Report

The report is structured in seven chapters that together will fulfill the thesis objective. Chapter 2 provides an introduction to the area of FACTS-devices and introduces several concepts in control theory that will be referred to in later chapters. The chapter also introduces fundamental concepts in control of voltage source converters. Chapter 3 further develops the concept of control of voltage source converters and introduces several grid forming control methods. Chapter 4 describes the two simulation models that were produced in order to investigate the grid-forming behavior. Chapter 5 presents the simulation results and briefly describes the consequences of these results. Chapter 6 provides a further discussion on the implications of the results and provides an answer to the questions that the thesis seeks to answer. Chapter 7 presents the conclusions of the thesis.

Chapter 2

Background

The following chapter seeks to provide the reader with a theoretical background regarding concepts used in later chapters. The chapter starts with an introduction to the area of FACTS-devices and properties of STATCOM-systems. Thereafter, a theoretical background of control theory such as transfer functions, state space representations and stability assessments is presented to form a basis for the investigation of converter stability. The chapter is concluded with a section explaining some of the fundamental elements in the control of voltage source converters (VSCs). Chapter 3 will then further investigate different control methods. This chapter introduces the concepts at a general level, for a more in depth understanding the reader is referred to the specified literature.

2.1 FACTS-devices

IEEE defines Flexible AC Transmission Systems (FACTS) as “alternating current transmission systems incorporating power-electronic based and other static controllers to enhance controllability and increase power transfer capability” [7]. These controllers can be placed in a shunt configuration in order to provide voltage and reactive power control or in series for active power flow control [8]. Other benefits of FACTS-devices are, for example, enhanced system damping, improved transient stability and limited short circuit current. Different FACTS-devices can introduce different system benefits due to their different topologies. It is common to classify the devices into the following categories [9]:

1. Thyristor-based
 - (a) Static Var Compensator (SVC)
 - (b) Thyristor-Controlled Series Compensation (TCSC)
2. Voltage-source converter (VSC)-based
 - (a) Static Synchronous Compensator (STATCOM)
 - (b) Static Synchronous Series Compensator (SSSC)
 - (c) Unified Power Flow Controller (UPFC)

This study focuses on the STATCOM which use voltage source converter (VSC) technology. A VSC uses a capacitor connected to active switches to impose a voltage at its terminal. The capacitor is used as a voltage source, hence the term voltage source converter. Active switches are realized using insulated-gate bipolar transistors (IGBTs) or switches with similar capabilities. In this application the VSC is used to generate AC-voltage from a DC-source. With the converter it is possible to control the phase, frequency and magnitude of the output voltage. In Figure 2.1 an example of a basic VSC is displayed, namely the three phase two level VSC.

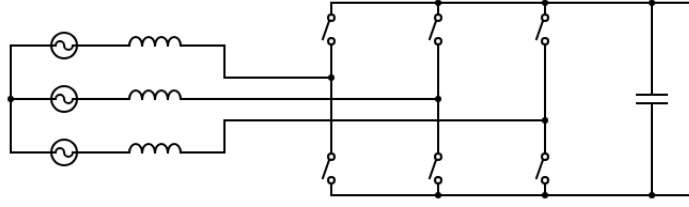


Figure 2.1: A grid connected three-phase two-level VSC displayed with generic switches.

By modulating the switch states, it is possible to convert the DC-voltage to AC. The DC-voltage has a fixed polarity and utilizes a large enough capacitor in order to provide a stable DC-voltage. In order to reverse the power flow through the converter the polarity of the current is reversed [10].

In order for the VSC to provide reactive power to the grid, the magnitude of the converter output voltage is increased above the grid voltage and reduced below the grid voltage in order to consume reactive power. By changing the phase angle of the output voltage it is also possible to achieve an active power flow, this presumes that the DC-side is connected to a DC energy storage e.g. supercapacitors or a battery energy storage system [8].

Utility scale STATCOM-systems are built on the principle of modular multi-level converters (MMC). However, the basic principles of the VSC are still used and hence it can be modelled as an average voltage source converter. MMCs has several benefits over more conventional VSC topologies such as lower switching losses and a reduced harmonic content. In a MMC-system one single switch in Figure 2.1 is replaced with a large number of switches connected in series, creating one valve. Each valve consists of several submodules, were each submodule contains one capacitor. This makes it possible for each valve to act as a voltage source. For more details on modular multi-level converters the reader are referred to [11] and [12].

2.2 Transfer Functions, System Response & State Space Models

In this study, transfer functions and state space models are used to model the behavior of the VSC and its control system. In control theory it is common to describe how the output signal of a linear system is affected by the input signal by using transfer functions and hence establish an input/output-signal relation. These transfer functions can be obtained by applying Laplace transform on the differential equations that describes the system behavior. Such a differential equation, with input signal u and output signal y , is illustrated in (2.1) where $y^{(n)}(t)$ denotes the n'th time derivative of $y(t)$

$$y^{(n)}(t) + a_1y^{(n-1)}(t) + \dots + a_ny(t) = b_0u^{(n)}(t) + b_1u^{(n-1)}(t) + \dots + b_nu(t). \quad (2.1)$$

An input/output relation can be formed by applying a Laplace transform on (2.1)

$$Y(s) = \frac{B(s)}{A(s)}U(s) = H(s)U(s), \quad (2.2)$$

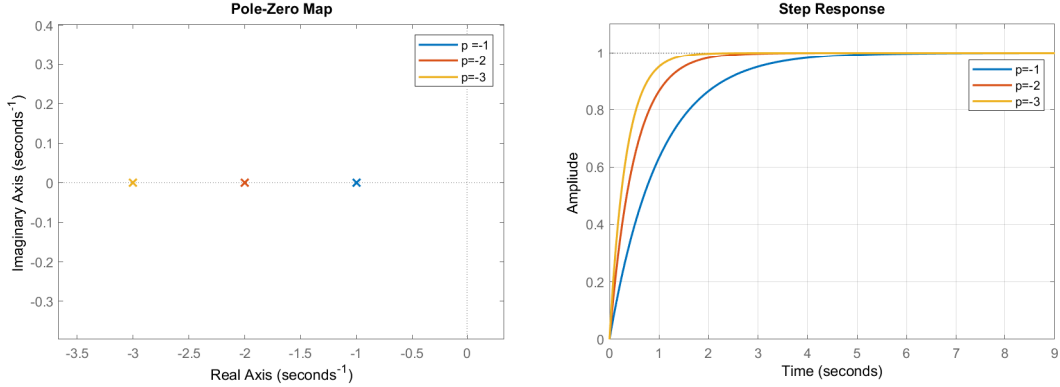
where $A(s)$ and $B(s)$ are polynomials in s and the ratio $\frac{B(s)}{A(s)}$ forms the transfer function $H(s)$. The roots to the denominator polynomial of the transfer function, $A(s)$, are known as *poles*, and the roots to the numerator polynomial, $B(s)$, are known as *zeros* [13].

The location of the poles characterizes the dynamic behavior of the system. For a continuous-time system, the poles should be located in the left half plane of the complex plane (a negative real part) for the system to be stable. Stability is characterised by the impulse response of the system goes to zero as time goes to infinity [13].

It can be shown that poles placed closer to the origin slows down the response of the system and if the pole is placed with a positive real part the system is unstable. This behavior can be illustrated with the following first order system,

$$H(s) = \frac{1}{1 + Ts} \quad (2.3)$$

where T is a time constant. Figure 2.2 shows a step response and a pole-zero plot of the system described by (2.3) where T is chosen to place the poles at $-3, -2$ and -1 (equivalent to $T = 1, T = 1/2$ and $T = 1/3$).



(a) Pole-zero plot of the system in (2.3) where T is chosen to place the poles at $-3, -2$ and -1 . (b) Step response of (2.3) with poles placed at $-3, -2$ and -1 .

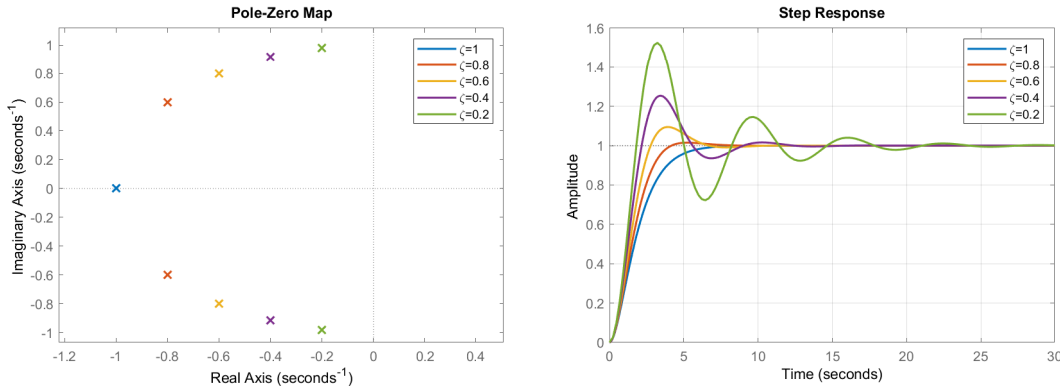
Figure 2.2: Pole-zero map and step response of the system described by (2.3). Note that p is used to denote the pole location in this figure.

Figure 2.2 illustrates that poles placed further away from the origin gives a faster response. (2.3) describes a first order system.

For a second order system the poles will appear in complex conjugate pairs and the imaginary part of the pole location will influence the system damping. For the second order system

$$H(s) = \frac{\omega^2}{s^2 + 2\xi\omega s + \omega^2}, \quad (2.4)$$

changing the constant $0 < \xi < 1$ will alter the damping performance. This is illustrated in Figure 2.3.



(a) Pole-zero plot of the system in (2.4) where ξ varies between 1 and 0.2 and for $\omega = 1$. (b) Step response of (2.4) where ξ varies between 1 and 0.2 and for $\omega = 1$.

Figure 2.3: Pole-zero map and step response of the system described by (2.4).

Keeping ω constant and varying ξ places the poles on a circle with constant radius. This illustrates that ω governs the pole distance from the origin while ξ determine at what angle, seen from the real axis, the pole is placed. It can also be concluded from Figure 2.3 that the overshoot reduces with increased damping i.e. larger ξ . It is therefore desired to place poles as close to the real axis as possible [13].

Lastly, the concept of pole-zero cancellation is shortly introduced. If one or several zeros matches poles of the system, the zeros can cancel the system poles and hence remove their properties from the overall system response. This is true in theory but can be hard to accomplish in practice since small mismatches between the pole and zero are likely. Pole zero cancellation should therefore rather be used as a convenient concept to assess system behavior than an exact design tool[13].

2.2.1 State Space Representation

State space representations is another way to represent the differential equations that describe a system, based on vector and matrix notation. A state is defined as the information needed in order to foresee the effect of a certain input signal. Consider the system 2.5

$$\ddot{y}(t) + a_1\ddot{y}(t) + a_2\dot{y}(t) + a_3y(t) = bu(t). \quad (2.5)$$

It is possible to write this differential equation as a system of first order equations using

$$\begin{aligned} x_1(t) &= y(t) \\ x_2(t) &= \dot{y}(t) \\ x_3(t) &= \ddot{y}(t). \end{aligned} \quad (2.6)$$

The x -variables can now be derived to

$$\begin{aligned} \dot{x}_1(t) &= \dot{y}(t) = x_2(t) \\ \dot{x}_2(t) &= \ddot{y}(t) = x_3(t) \\ \dot{x}_3(t) &= \ddot{\ddot{y}}(t) = -a_1\ddot{y}(t) - a_2\dot{y}(t) - a_3y(t) + bu(t) \\ &= -a_1x_3(t) - a_2x_2(t) - a_3x_1(t) + bu(t), \end{aligned} \quad (2.7)$$

and if matrix notation is applied

$$\begin{bmatrix} \dot{x}_1(t) \\ \dot{x}_2(t) \\ \dot{x}_3(t) \end{bmatrix} = \underbrace{\begin{bmatrix} 0 & 1 & 0 \\ 0 & 0 & 1 \\ -a_3 & -a_2 & -a_1 \end{bmatrix}}_A \begin{bmatrix} x_1(t) \\ x_2(t) \\ x_3(t) \end{bmatrix} + \underbrace{\begin{bmatrix} 0 \\ 0 \\ b \end{bmatrix}}_B u(t). \quad (2.8)$$

By establishing the row vector

$$C = [1 \ 0 \ 0], \quad (2.9)$$

(2.7) and (2.8) can now be written as

$$\begin{aligned} \dot{x}(t) &= Ax(t) + Bu(t) \\ y(t) &= Cx(t) + Du(t) \end{aligned} \quad (2.10)$$

which is the general state space representation of a linear system. The poles of a system written on state space form can be obtained by solving the following equation

$$\det(sI - A) = 0, \quad (2.11)$$

were I is the identity matrix and s is a complex variable in the Laplace domain. This implies that the eigenvalues of A , corresponds to the system poles. Hence, if the eigenvalues are located in the left half plane the system is stable. The pole locations can be further analysed by computing its natural frequency and damping factor. The natural frequency of a pole is the frequency that the system would oscillate with if there is no damping and the damping factor relates to how well these oscillations are damped [13], [14].

2.2.1.1 Participation Factors

Previously, a description on how the eigenvalues i.e. the poles can be analyzed in order to understand the system dynamics was provided. However no information is obtained on how the poles relates to the different states that forms the state space representation. For that purpose the tool of participation factors can be applied. The calculation of participation factors uses the right and left eigenvector of the A -matrix to provide a measure of the relative participation between states and poles. The left and right eigenvectors of the state space matrix is obtained by

$$A\Phi = \lambda\Phi \quad (2.12)$$

$$\Psi = (\Phi^{-1})^T, \quad (2.13)$$

where λ are the eigenvalues of the state matrix, Φ is the right eigenvector and Ψ the left eigenvector. In [15] the participation factor is defined as

$$PF_{ki} = (\Phi \circ \Psi)_{ki} = \begin{bmatrix} \Phi_{11}\Psi_{11} & \dots & \Phi_{1i}\Psi_{i1} \\ \vdots & \ddots & \vdots \\ \Phi_{k1}\Psi_{1k} & \dots & \Phi_{ki}\Psi_{ik} \end{bmatrix} \quad (2.14)$$

where PF_{ik} is the participation factor that provides a “measure of the relative participation of the k th state variable in the i th mode, and vice versa” [15].

2.3 Reference Frames used in the Control of VSCs

To be able to create state space models of the STATCOM-circuit and control system for simulations, the properties of the control system needs to be identified. Active control is needed to regulate the output voltage and current of a voltage source converter to a desired value. Since VSCs are implemented as three-phase systems, in order to have total control over the current it would be necessary to track three sinusoidal current waveforms. However, by the internal model principle, tracking sinusoidal waveforms is complicated and would require a resonant controller. The design of such compensators is not straightforward. Another more common solution to the control problem is a change of reference system using the two reference systems referred to as the $\alpha\beta$ -frame and the dq-frame. This enables the use of standard PI-controllers that are significantly easier to design and have proven to be robust as they are extensively used in industry [16].

2.3.1 The $\alpha\beta$ -frame

A symmetric and balanced three-phase system can be described as

$$\begin{aligned} f_a(t) &= \hat{f} \cos(\omega t + \theta_0), \\ f_b(t) &= \hat{f} \cos(\omega t + \theta_0 - \frac{2\pi}{3}), \\ f_c(t) &= \hat{f} \cos(\omega t + \theta_0 - \frac{4\pi}{3}), \end{aligned} \quad (2.15)$$

where \hat{f} is the amplitude, θ_0 the initial phase angle and ω the angular frequency. The functions in (2.15) can be written as one state phasor, defined as (where i is the imaginary unit that satisfies $i^2 = -1$)

$$\vec{f}(t) = \frac{2}{3} \left[e^{i0} f_a(t) + e^{i\frac{2\pi}{3}} f_b(t) + e^{i\frac{4\pi}{3}} f_c(t) \right]. \quad (2.16)$$

Now, $\vec{f}(t)$ can be decomposed into its real and imaginary parts

$$\vec{f}(t) = f_\alpha(t) + i f_\beta(t). \quad (2.17)$$

where α is the real and β is the imaginary component. Equating the real and complex parts of (2.16) and (2.17) results in the following signal transformation

$$\begin{bmatrix} f_\alpha(t) \\ f_\beta(t) \end{bmatrix} = \frac{2}{3} \begin{bmatrix} 1 & -\frac{1}{2} & -\frac{1}{2} \\ 0 & \frac{\sqrt{3}}{2} & -\frac{\sqrt{3}}{2} \end{bmatrix} \begin{bmatrix} f_a(t) \\ f_b(t) \\ f_c(t) \end{bmatrix}. \quad (2.18)$$

This can be seen as a projection of (2.15) on the real and imaginary axis. Since $\vec{f}(t)$ is a space vector rotating with the grid frequency the value of the α - and β -components will change in time. The α -vector will vary along the real-axis and β will vary along the imaginary axis, hence the α - and β - will behave as

$$\begin{aligned} f_\alpha(t) &= \hat{f}(t)\cos(\theta(t)) \\ f_\beta(t) &= \hat{f}(t)\sin(\theta(t)), \end{aligned} \quad (2.19)$$

where $\theta(t)$ is the phase angle of the grid. This transformation into the $\alpha\beta$ -frame has reduced the system of three components into two components. But, the signals still behaves as sinusoidal signals, to solve this problem an additional transformation into the rotating dq -frame is introduced [16].

2.3.2 The dq-frame

The dq-frame presents a solution to the problem of oscillating control signals and transforms them into DC-waveforms during steady-state conditions. This is possible by rotating the $\alpha\beta$ -reference frame with the frequency of the AC-signals. This can be mathematically formulated as

$$\vec{f}(t) = f_d(t) + i f_q(t) = (f_\alpha + i f_\beta)e^{-i\varphi(t)} \quad (2.20)$$

and can be seen as a phase shift with an angle $\varphi(t)$. Using Euler's identity $e^{ix} = \cos(x) + i\sin(x)$ (2.20) can be rewritten as

$$\begin{bmatrix} f_d(t) \\ f_q(t) \end{bmatrix} = \begin{bmatrix} \cos(\varphi) & \sin(\varphi) \\ -\sin(\varphi) & \cos(\varphi) \end{bmatrix} \begin{bmatrix} f_\alpha(t) \\ f_\beta(t) \end{bmatrix}. \quad (2.21)$$

Combining the two transformations results in a direct transformation from abc -frame to dq -frame [16]

$$\begin{bmatrix} f_d(t) \\ f_q(t) \end{bmatrix} = \frac{2}{3} \begin{bmatrix} \cos(\varphi(t)) & \cos(\varphi(t) - \frac{2\pi}{3}) & \cos(\varphi(t) - \frac{4\pi}{3}) \\ \sin(\varphi(t)) & \sin(\varphi(t) - \frac{2\pi}{3}) & \sin(\varphi(t) - \frac{4\pi}{3}) \end{bmatrix} \begin{bmatrix} f_a(t) \\ f_b(t) \\ f_c(t) \end{bmatrix}. \quad (2.22)$$

Figure 2.4 shows the result of a three-phase voltage waveform being transformed into the $\alpha\beta$ - and dq -frame. Note that the $\alpha\beta$ - and dq -frame are also commonly known as the stationary and rotating frame.

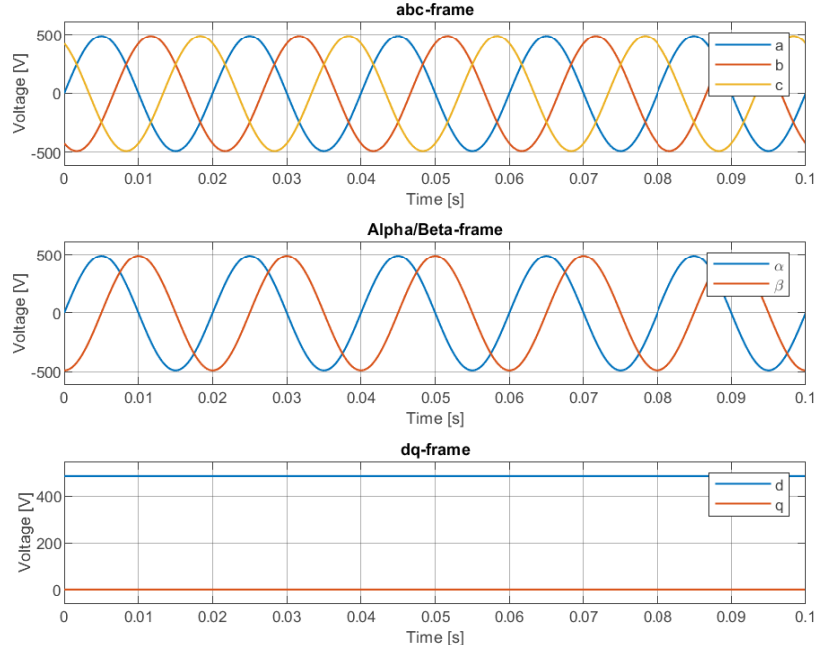


Figure 2.4: Transformation of a three-phase voltage waveform into the $\alpha\beta$ - and dq -frame.

It can be shown that the active and reactive power in the dq-frame can be calculated with the following relations

$$P(t) = \frac{3}{2}[v_d(t)i_d(t) + v_q(t)i_q(t)] \quad (2.23)$$

$$Q(t) = \frac{3}{2}[-v_d(t)i_q(t) + v_q(t)i_d(t)]. \quad (2.24)$$

If $v_q(t)$ is zero, which often is the case for a grid connected VSC in steady state (an explanation of why this is the case follows in Section 3.1.1), active power is proportional to i_d and the reactive power to i_q [16].

In this section two reference systems for VSC control have been introduced. These reference frames forms a basis for controlling VSC and they are implemented in control methods described in the following chapter.

Chapter 3

VSC Control Modes

Voltage source converters (VSCs) can be controlled in several different ways and hence display different behaviors. A variety of classification methods can be found in literature, in this study the methodology proposed by [5] and further developed by [2] will be used.

Depending on the operational mode, converters can be classified as *grid-forming*, *partial grid-forming* or *grid-following* (also known as grid-feeding) [2]. This study will mainly focus on grid forming control but also make comparisons with partial grid-forming and grid-following control methods.

3.1 Grid-Following Control

A grid-following VSC acts as a current source which inject active and reactive power to the grid according to defined power, or current setpoint. Most of the converters used today are of the grid following type. In order to inject power to the grid, the control structure must first synchronize with the grid using a PLL that measures the angle of the grid voltage. The overall control structure usually consists of an outer voltage control loop that generates reference values for the inner current control loop. The current loop therefore needs to be fast in its control while the voltage loop can be slower [5]. In Figure 3.1 a schematic overview of a grid following control method is displayed.

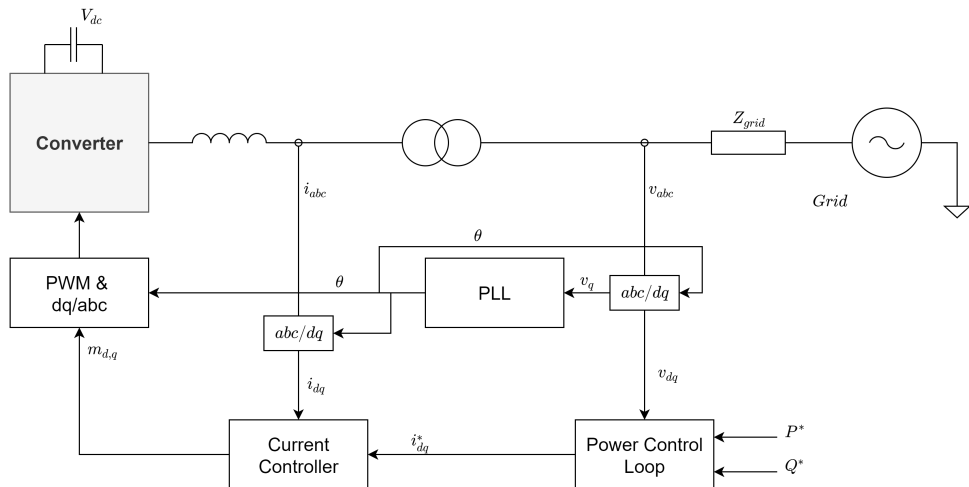


Figure 3.1: Illustration of a grid-following control method.

3.1.1 Grid-Following Synchronization

In order to use the dq-transformation in the control of a VSC converter, information regarding the grid frequency is needed in order to apply the abc/dq-transformation. For the transformation to function properly the rotation of the reference system must match the frequency of the AC-signals. The PLL serves the purpose of providing the correct phase angle and frequency to the dq-transformation making it possible to synchronize the VSC to the grid with grid-following control [16].

The voltages V_d and V_q can be written as

$$V_d(t) = \hat{V} \cos(\omega t + \theta_0 - \varphi) \quad (3.1)$$

$$V_q(t) = \hat{V} \sin(\omega t + \theta_0 - \varphi) \quad (3.2)$$

where φ is the rotation of the dq-frame. If synchronized, $\varphi = \omega t + \theta_0$ and it can be observed from (3.2) that $V_q = 0$. Therefore, regulating the V_q voltage to zero can be used to provide the correct rotation to the dq-transformation. This can be formulated in a feedback law as,

$$\omega = H(s)V_q(t), \quad (3.3)$$

where $H(s)$ is a linear transfer function and can be implemented as a PI-regulator. When ω is obtained one must go from ω to φ and since $\frac{d\varphi}{dt} = \omega$ an integrator is needed. This integrator is implemented as a voltage-controlled oscillator (VCO) and can be seen as a wrapped state integrator that limits its output between 0 and 2π and resets the output to zero when 2π is reached [16].

Figure 3.2 shows an implementation of the PLL and how it provides the correct rotation to the abc-dq-transformation.

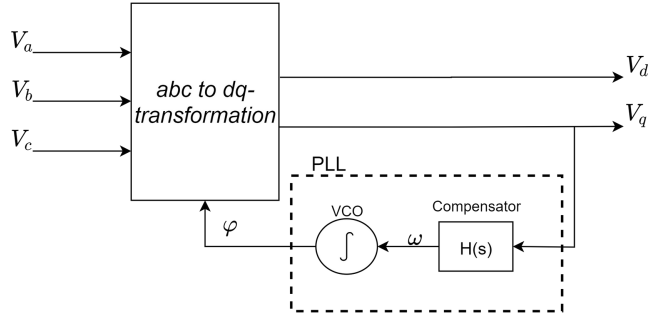


Figure 3.2: A schematic diagram of a PLL implemented in an abc-dq-transformation.

3.2 Grid-Forming Control

In grid-forming control the converter is controlled in order to behave as an AC voltage source with a specified voltage amplitude, phase and frequency. A VSC operating with grid-forming control can therefore be seen as a controllable AC-voltage source behind a coupling reactance, similar to a synchronous generator. What differentiates grid-forming from grid-following is mainly the synchronization method that provides the correct rotation in the abc/dq-transformation. In grid-forming control this synchronization is based on the concepts of active power transfer and the swing equation [5]. A generic grid forming control method is illustrated in Figure 3.3.

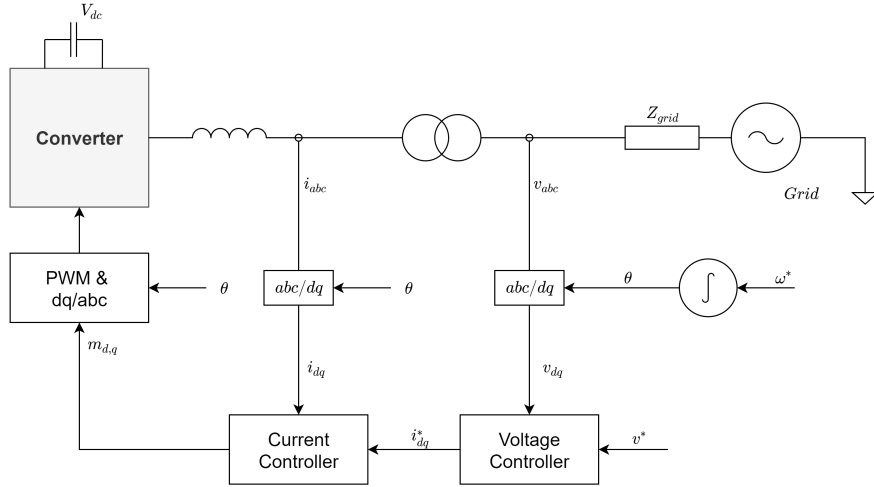


Figure 3.3: Illustration of a generic grid-forming control method.

Partial grid-forming control is based on grid-forming control but implements only a voltage forming behavior. With a voltage forming control method the voltage amplitude at the PCC is set with a reference value and a phase locked loop is used to synchronize to the grid [2].

To further introduce the desired frequency behavior and characteristics of the synchronous machine, the following section will establish further insights in the behavior of synchronous machines and the swing equation. The section also describes how the concept of stability is defined in a power system context and the governing quantities of active and reactive power.

3.2.1 The Swing Equation and Power Transfer Equations

The concept of power system stability is associated with two concepts, rotor angle and voltage stability. Rotor angle stability considers the ability of all synchronous machines in an area to remain in synchronism, while voltage stability considers the ability of a power system to maintain acceptable voltage levels [15].

A synchronous machine consists of a rotor that provides a rotating magnetic field and a stator that holds the armature windings. When the rotor is set in motion by a prime mover (such as a hydro power turbine) the rotating magnetic field on the rotor will result in induced voltage in the stator armature windings. The frequency of this induced voltage, and of the current that will flow in case the stator is connected to a load, is determined by the rotating frequency of the rotor. Hence the electric frequency of the stator is synchronized with the rotor speed. Since the frequency of the power system is fixed at 50 or 60 Hz depending on local grid codes, the electric frequency of the output voltage and current of all synchronous machines in a power system must be equal (in steady state). This also implies that all synchronous machines must rotate so that the same electrical frequency is generated. The electrical output torque is changed by changing the mechanical torque applied by the prime mover. This will advance the angular position of the rotor relative to the stator field. The torque balance of the generator during an unbalance in torque will result in an acceleration or deceleration and can be written as

$$T_a = T_m - T_e \quad (3.4)$$

where T_a is the accelerating torque while T_m and T_e is the mechanical and electrical torque applied. The electrical torque is a result from an applied load, either a local one or applied by the grid. Considering that the rotor is a rigid body with considerable mass, the accelerating torque in (3.4) can be written as

$$J \frac{d\omega}{dt} = T_m - T_e, \quad (3.5)$$

where J is the combined moment of inertia of the generator and turbine, ω is the angular velocity of the rotor and t represents time. This equation is commonly known as the swing equation. It is common to

write the swing equation on a per unit base where the total moment of inertia, J , often is denoted as a per unit quantity by H ,

$$H = \frac{1}{2} \frac{J\omega^2}{S_{base}} \quad (3.6)$$

where S_{base} is the system power base.

To further describe the dynamics of the swing equation, consider that a large increase in load occurs for a synchronous generator. The electrical torque will consequently increase. If the mechanical energy on the generator shaft remains constant, this increase in load torque will take energy from the kinetic energy stored in the rotating mass and will thus cause the generator to decelerate and thus lower the mechanical speed of the rotor. It is possible to compensate this deceleration by increasing the torque on the generator shaft. [15].

Power Transfer Equations

From the previous paragraph it can be noted that an angle advancement of the bus voltage corresponds to a transfer of active power. This will be further explained in this section. Consider the power transfer in a two bus system, as illustrated in Figure 3.4.

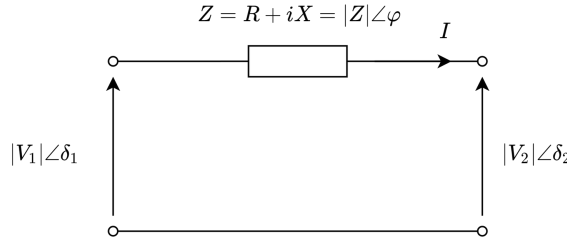


Figure 3.4: Power transfer across an impedance.

The complex power, S , flowing through the impedance can be written as

$$S = P + jQ \quad (3.7)$$

where P denotes active power and Q reactive power. The current I is according to Ohm's law

$$I = \frac{|V_1|\angle\delta_1 - |V_2|\angle\delta_2}{|Z|\angle\varphi}. \quad (3.8)$$

The complex power at node 2 (in Figure 3.4) can be calculated as,

$$\begin{aligned} S &= V_2 I^* = |V_2|\angle\delta_2 \cdot \frac{|V_1|\angle-\delta_1 - |V_2|\angle-\delta_2}{|Z|\angle(-\varphi)} \\ &= \frac{|V_1||V_2|\angle(\delta_2 - \delta_1) - |V_2|^2\angle0}{|Z|\angle-\varphi} \\ &= \frac{|V_1||V_2|}{|Z|}\angle(\varphi + \delta_2 - \delta_1) - \frac{|V_2|^2}{|Z|}\angle(\varphi). \end{aligned} \quad (3.9)$$

where I^* denotes the complex conjugate to I . By acknowledging that the active power is the real part of S and that the reactive power is the complex part, it can be deduced that

$$\begin{aligned} P &= \frac{|V_1||V_2|}{|Z|}\cos(\varphi + \delta_2 - \delta_1) - \frac{|V_2|^2}{|Z|}\cos(\varphi) \\ Q &= \frac{|V_1||V_2|}{|Z|}\sin(\varphi + \delta_2 - \delta_1) - \frac{|V_2|^2}{|Z|}\sin(\varphi). \end{aligned} \quad (3.10)$$

At this point it can be noted that the X/R-ratio commonly is large for high voltage systems, this validates the assumption that $R \ll X$, therefore the resistive part of Z can be neglected, giving $Z = |Z|\angle\varphi =$

$X\angle\pi/2$. Also, the voltage angle difference is regularly small, validating the assumption that $\sin(\delta_1 - \delta_2)$ can be replaced by $\delta_1 - \delta_2$ and $\cos(\delta_1 - \delta_2)$ by 1. This gives,

$$\begin{aligned} P &= \frac{|V_1||V_2|}{X} \sin(\delta_1 - \delta_2) = \frac{|V_1||V_2|}{X} (\delta_1 - \delta_2) \\ Q &= \frac{|V_1||V_2|}{X} \cos(\delta_1 - \delta_2) - \frac{|V^2|}{X} = \frac{|V_2|}{X} (|V_1| - |V_2|). \end{aligned} \quad (3.11)$$

From (3.11) it is important to note that the active power is governed by the bus angle difference and that the reactive power is dependent on the voltage magnitude. Hence, the bus angle can be used to control the active power flow and the difference in voltage magnitude can be used to control reactive power flow. Alternatively, active power can be used to control the bus angle and reactive power can be used to control the voltage magnitude [8].

These power transfer equations as well as the dynamics provided by the swing equation serves as the foundation in the formulation of grid-forming control methods. Three different grid forming control methods will be further described, namely the method of synchronous power control (SPC), Power synchronization control (PSC) and droop control. Initially their frequency behavior will be studied and thereafter a description of their voltage behavior will follow. Other grid forming methods have been presented in literature, but are not presented further in this study. A short description of such methods will be provided in Appendix B together with references for the interested reader.

3.2.2 Frequency Behavior

The frequency behavior is essential for the converter to be able to perform fast frequency response services and show a frequency forming behavior. The following sections will in detail describe how the grid synchronization is performed.

3.2.2.1 Synchronous power control (SPC)

SPC is the control method with the implementation that is closest to the swing equation of the three different methods but it is not a direct implementation.

Initially an illustration of the concept of synchronization via transient power transfer will be provided. Assume that there are two synchronous generators in a power system. If machine one experiences an increased mechanical torque during a short time, according to the swing equation this will cause the rotor of machine one to rotate faster, increase the internal EMF of machine one and a phase advancement of the EMF will be seen. According to (3.11) this results in an increase in electric power sent from machine one to machine two. This causes an acceleration of the rotor in machine two and the phase difference between the two machines decreases. After a transient period, the phase difference between the machines are reset to the original and steady state is reached. This example shows that a speed difference, or in reality, a difference in the angular rotor position, will cause the other machine to follow in order to preserve synchronism [15].

The synchronization and active power loop are designed as an emulation of the swing equation of synchronous machines, here written in terms of power instead of torque and in the Laplace domain instead of the time domain,

$$P_m - P_e = \left(\frac{2HS_N}{\omega_s} s + D \right) \omega \quad (3.12)$$

where P_m and P_e is the mechanical and electrical power, H describes the inertia constant, S_N is the nominal power of the generator, ω_s and ω the nominal and output angular speed and D is the damping factor. With grid connected converters it is more interesting to write (3.12) on the form

$$\omega = \omega^* + \frac{1}{(2HS_N/\omega_s)s + D} (P^* - P) \quad (3.13)$$

where P^* is the active power reference. In [17] a generalised form of (3.13) is implemented that incorporates the inertia emulation and a power-frequency droop behavior. The implemented structure, similar

to (3.13) is

$$\omega = \omega^* + \frac{K_p s + K_i}{s + K_g} (P^* - P) \quad (3.14)$$

where the parameters K_p , K_i and K_g can be set to govern the damping, inertia and droop characteristics respectively, and can be derived to

$$K_i = \frac{\omega_s}{2HS_N}, \quad (3.15)$$

$$K_g = \frac{1}{2HR_d} \quad (3.16)$$

where R_d is the slope of the droop-curve, H is the inertia factor and

$$K_p = 2\xi\sqrt{\frac{\omega_s}{2HS_N P_{max}}} - \frac{1}{2HR_d P_{max}} \quad (3.17)$$

where ξ is the damping factor [17]. This is an implementation that lies close to the swing equation and incorporates several of the synchronous machine characteristic properties. A method that uses a more scaled downed version of the swing equation is the power synchronization control (PSC)-method.

3.2.2.2 Power-Synchronization Control (PSC)

Power-Synchronization Control (PSC) is similar to the synchronous power control (SPC) since they both are based on the behavior of the swing equation. But PSC scales down the implementation and disregards the use of inertia constants, droop factors and damping constants. PSC is based on the illustrative example provided in the beginning of section 3.2.2.1, where synchronization is provided based on transfer of active power. With that in mind, the power-synchronization loop is implemented as

$$\omega = \omega^* + \frac{K_p}{s} (P^* - P), \quad (3.18)$$

where the power control error is integrated to an angle error that is added to the frequency reference, ω^* . ω is then used to supply the angle for the abc/dq-transformations [18].

3.2.2.3 Droop Control

Droop control is the simplest implementation of the swing equation. Where the main idea is to measure the active and reactive power and use changes in the measured power flow in order to provide setpoints to a voltage and current controller. Droop control has historically been implemented in micro grids where it introduced the possibility for several converters to operate in parallel and together form the grid [19], [20]. Droop control have therefore been used more extensively compared to the newer control methods like SPC and PSC.

The synchronization is based on droop characteristics where the converter output frequency is linearly adjusted according to changes in the active power flow. This can be formulated as

$$\omega = \omega^* - mP \quad (3.19)$$

where ω^* is the nominal frequency and m is a droop gain. Figure 3.5 illustrates the droop behavior. If the active power transfer is zero the reference frequency is applied, but if there is a positive output power transfer, the converter frequency is reduced in order to reduce this power transfer and restore synchronism [21].

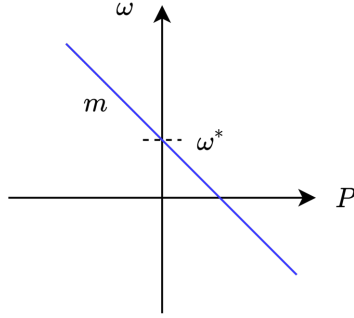


Figure 3.5: Graphical representation of the droop law in (3.19)

One could also modify (3.19) by instead applying the droop gain on $P_{error} = P^* - P$, giving the following droop equation

$$\omega = \omega^* - m(P^* - P) \quad (3.20)$$

where P^* is the nominal power. It is possible to apply the same principles as explained above on the reactive power control. By adding a droop gain on the measured reactive power, the voltage amplitude can be adjusted in order to control the reactive power flow.

$$v_{pcc} = v_{pcc}^* - nQ \quad (3.21)$$

where v_{pcc}^* is the nominal output voltage and n is a static droop gain. The static droop gains m and n can be formulated in the following way [21],

$$m = \frac{\omega_{max} - \omega_{min}}{P_{max}} \quad (3.22)$$

$$n = \frac{v_d \ max - v_d \ min}{Q_{max}}. \quad (3.23)$$

3.2.3 Voltage Behavior

Proper voltage behavior is important to be able to cope with possible grid disturbances and to provide a stable voltage output. The voltage behavior also makes the frequency behavior possible. In the following sections the voltage behavior of the introduced control methods will be described.

3.2.3.1 Synchronous Power Control (SPC)

The control actions of the SPC method is actuated in the $\alpha\beta$ -frame and uses a virtual admittance structure in order to generate reference values to a current controller. The setpoints to the virtual admittance structure can be set manually or using a Q-V droop controller. The Q-V droop controller is used to regulate the voltage level and hence control the reactive power. The reactive power reference is set by

$$Q^* = Q_{set} + D_Q(V^* - V) \quad (3.24)$$

where Q_{set} is a setpoint for the reactive power transfer and D_Q is a droop coefficient. Q^* is then used in the reactive power controller with the following PI-structure

$$V = V^* + \left(K_{pQ} + \frac{K_{iQ}}{s} \right) (Q^* - Q). \quad (3.25)$$

V is thereafter used as an amplitude voltage to generate the α and β -voltage reference

$$v_\alpha^* = V \cos(\omega t) \quad (3.26)$$

$$v_\beta^* = V \sin(\omega t) \quad (3.27)$$

where ωt is obtained from the synchronization loop. The SPC-method uses a virtual admittance to generate reference currents to the current controller rather than a standard voltage regulator. The virtual admittance gives the benefits of current limitation as well as ensuring a high X/R ratio. By introducing a virtual admittance instead of a real one, power losses and bulky components are avoided since no physical components are implemented. In single phase the virtual admittance is implemented as

$$i_{\alpha,\beta}^* = \frac{v_{\alpha,\beta}^* - v_{\alpha,\beta}}{R_v + sL_v}, \quad (3.28)$$

where L_v is a virtual inductance and R_v a virtual resistance whereas $v_{\alpha,\beta}$ is the measured $\alpha\beta$ -voltages at the PCC. The current controller can be formulated in the stationary frame, formulated as

$$m_{\alpha,\beta} = \frac{1}{v_{dc}} \left(K_{p,i} + K_r \frac{\omega s}{s^2 + \omega^2} \right) (i_{\alpha,\beta}^* - i_{\alpha,\beta}). \quad (3.29)$$

where $m_{\alpha\beta}$ is the modulation signals sent to the pulse width modulation (PWM) generator [17].

Figure 3.6 displays an overall layout of the control structure, showing both the synchronization-loop as well as the voltage and current control.

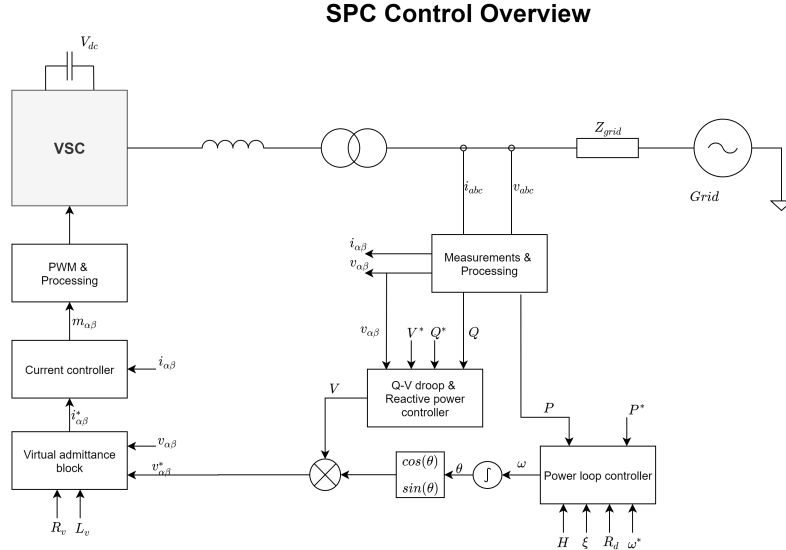


Figure 3.6: Illustration of the SPC-control method described by [17].

3.2.3.2 Power-Synchronization Control

The power-synchronization loop provide synchronism with the use of transient power flow. The current associated with this power flow is however unknown. Therefore, in [18], PSC is not implemented with a current controller since this requires a known current reference. Instead, the active power is controlled via the power-synchronization loop and the reactive power by varying the magnitude of the output voltage. For this reason, an inner current control loop is not required. In grid fault situations where the current grows significantly it will not be possible to limit the current and protect the converter valves against dangerous currents since there is no control of the current. Thus, [18] suggest that a back up system is to be implemented to handle such situations. The back-up system implements a PLL and a current controller [18].

The power reference, P^* , can be obtained from a DC-voltage controller (if it is necessary to control the DC-side voltage over the VSC) or by specifying the desired power reference. If a controller is desirable it can be implemented as

$$P^* = \left(K_{p,dc} + \frac{K_{i,dc}}{s} \right) \frac{(v_{dc}^*)^2 - v_{dc}^2}{2} \quad (3.30)$$

where $K_{p,dc}$ and $K_{i,dc}$ are PI-gains [18].

To control the voltage level at the PCC and hence the reactive power, it is possible to have a reactive power controller supplying a voltage reference to the AC-voltage controller. The reactive power controller is an ordinary PI-controller implemented on the control error, $Q^* - Q$, and the voltage reference is obtained using

$$u_{ac}^* = (Q^* - Q) \left(K_{pQ} + \frac{K_{iQ}}{s} \right), \quad (3.31)$$

where u_{ac}^* is used as an input to the AC-voltage controller, illustrated below

$$V_0 = v_0^* + \frac{K_E}{1 + T_E s} (u_{ac}^* - |v_{pcc}|), \quad (3.32)$$

where K_E and T_E are constants. The output of the controller, V_0 , is the voltage reference supplied to a current reference control that is needed in order to check if the current is dangerously large. This is especially important in grid fault situations where the current magnitude grow large and could exceed the rating of the converter. If so, the PLL and current control is applied in order to protect the converter. The voltage control law of the VSC is

$$m_{dq}^* = \alpha L(i_{dq}^* - i_{dq}) + j\omega L i_{dq} + u_{dq}^{ff} \quad (3.33)$$

where m_{dq}^* is the modulation signals in dq-space, α is the wanted closed-loop bandwidth of the current controller and u_{dq}^{ff} is a low-pass filtered feedforward term of the dq-voltages at the PCC. In (3.33) i_{dq}^* is given by

$$i_{dq}^* = \frac{1}{\alpha L} [V_0 - u_{dq}^{ff} - j\omega L i_{dq} - H_{HP}(s)i_{dq}] + i_{dq} \quad (3.34)$$

where $H_{HP}(s)$ is a high-pass filter. (3.34) and (3.33) are designed in such a way that for normal SPC-operation (3.33) becomes

$$m_{dq}^* = V_0 - H_{HP}(s)i_{dq} \quad (3.35)$$

where $H_{HP}(s)$ is a high-pass filter described by $H_{HP}(s) = \frac{k_v s}{s + \alpha_v}$. The use of (3.33) and (3.34) makes it possible to seamless switch between operation with the power-synchronization loop and the back-up PLL. The PLL-mode of operation is initiated if the current references obtained from (3.34) are larger than a specified value and i_{dq}^* are set to its maximum values [18].

Figure 3.7 shows an illustration of the above described PSC control method.

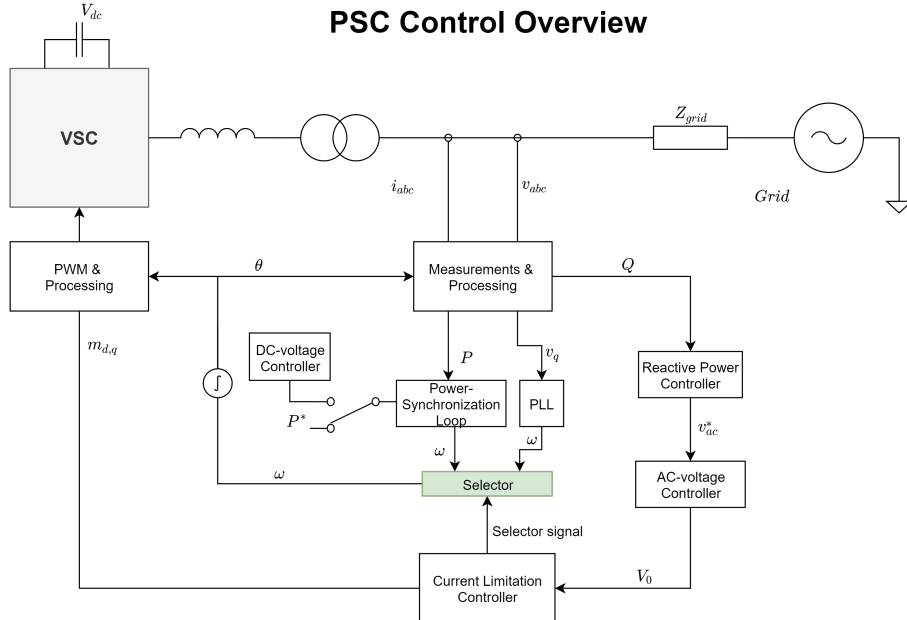


Figure 3.7: A graphical representation of the PSC-control method.

3.2.3.3 Droop Control

In order to control the voltage level according to the setpoints determined by the synchronization loops, a voltage controller is used to generate current setpoints (i_d^* and i_q^*) to a current controller. The voltage controller can for simplicity be implemented as a PI-regulator. Below the control structure from [21] where the control is implemented on a two level VSC with a LCL-filter is described. A two level VSC with a LCL-filter is displayed in Figure 3.8. The voltage controller is implemented as

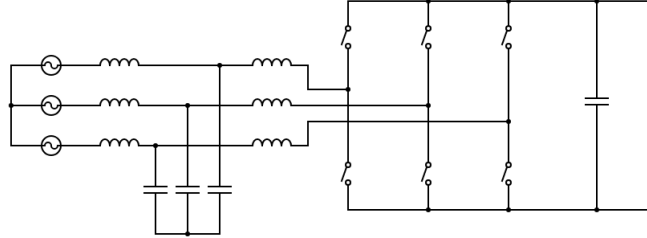


Figure 3.8: Two level VSC with a LCL-filter, used in [21].

$$i_d^* = \left(K_{pv} + \frac{K_{iv}}{s} \right) (v_d^* - v_d) - \omega C v_q + K_f i_d \quad (3.36)$$

$$i_q^* = \left(K_{pv} + \frac{K_{iv}}{s} \right) (v_q^* - v_q) - \omega C v_d + K_f i_q, \quad (3.37)$$

where K_{pv} and K_{iv} represents the PI-gains, K_f is a gain for the feedforward part and C the filter capacitance. The current controller is implemented in a similar way and is used to obtain a voltage vector for the PWM-generator. The dynamics of the controller can be described by

$$m_d = \left(K_{pi} + \frac{K_{ii}}{s} \right) (i_d^* - i_d) - \omega L i_q + v_d \quad (3.38)$$

$$m_q = \left(K_{pi} + \frac{K_{ii}}{s} \right) (i_q^* - i_q) + \omega L i_d + v_q \quad (3.39)$$

where K_{pi} and K_{ii} are the PI-gains of the current controller, L is the filter inductance and m_d , m_q are the modulation signals sent to the PWM-generator [21]. The described control structure is illustrated in Figure 3.9.

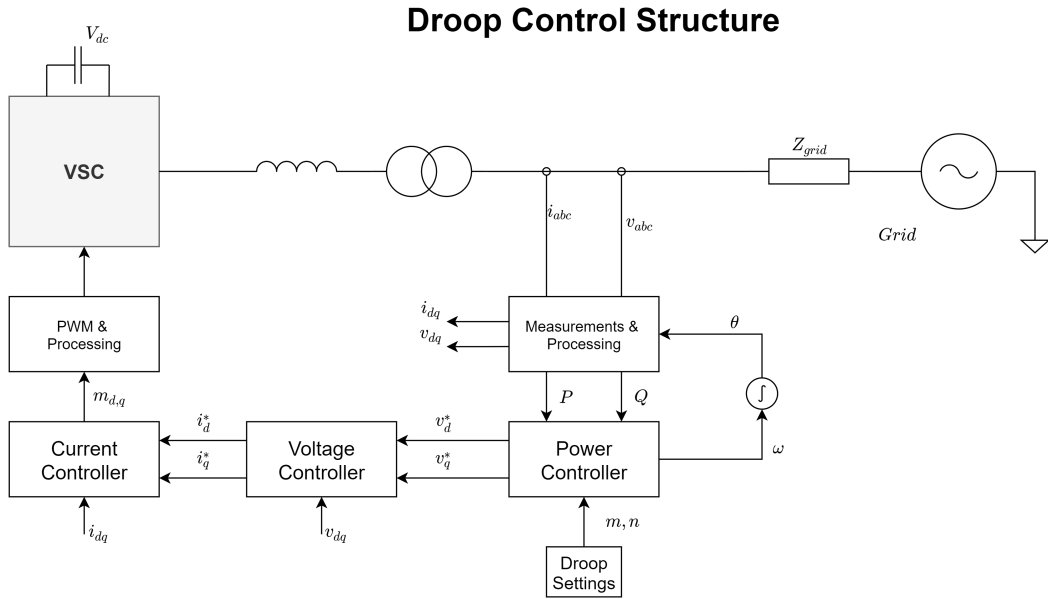


Figure 3.9: Principal layout of the droop control method.

There exist several variations of the droop control method with numerous adjustments and additions. For further insight in the concept of droop control the reader is referred to [22]–[26].

3.2.4 Summary and Discussion of Grid Forming Control Methods

There are several similarities between the different grid forming control methods that were presented in this chapter. Focusing on the synchronisation part of the control method, one can observe that they are all based on synchronization via active power transfer and the swing equation behavior. The synchronization-equation is summarized below:

- The Swing equation for the case of grid connected converters:

$$\omega = \omega^* + \frac{1}{(2HS_N/\omega_s)s + D}(P^* - P) \quad (3.40)$$

- SPC-synchronization:

$$\omega = \omega^* + \frac{K_p s + K_i}{s + K_q} (P^* - P) \quad (3.41)$$

- PSC-synchronization:

$$\omega = \omega^* + \frac{K_p}{s} (P^* - P) \quad (3.42)$$

- Droop-synchronization:

$$\omega = \omega^* - m(P^* - P) \quad (3.43)$$

The bullet list highlights the similarities between the different methods. The PSC synchronization could be seen as a developed droop synchronization where an integrator is added (a $\frac{1}{s}$ -term is equivalent to an integrator in the Laplace domain), changing the proportional feedback on the power error to an integrating one. Similarly, SPC could be seen as an even further developed version of the PSC-synchronization where additional dynamics is added. SPC synchronization is the method that comes closest to the original swing equation since it captures more of the system behavior since it incorporates e.g the inertia constant. Looking at the synchronization methods from a transfer function perspective on the power error illustrates that the PSC-method introduces a pole at 0 while the pole is shifted according to K_g in the SPC-method. Since droop only has a proportional part no pole is introduced. The location

of the poles is although not that straightforward to interpret since the dynamic of the control system will affect the transfer function from power to angle. It could however be noted that for K_p and $K_i = 0$ the SPC-synchronization is equivalent to the PSC one.

Looking at the voltage and current control, there are larger differences in how the control is actuated. The SPC-method is actuated in the stationary frame while PSC and droop control is performed in the rotating dq-frame. SPC uses a virtual admittance structure to calculate current setpoints to the current controller while droop control uses a traditional PI-regulator. Conversely, the PSC-method do not implement a current controller. Since grid-forming control implies that we have a controllable voltage source there is no needed for a current controller to obtain the desired voltage behavior. The downside of not implementing a current controller is however that it is not possible to limit the converter current, especially critical in grid fault situations.

The analysis in the following chapters will be limited to one of these control methods in order to limit the scope of the study. Since SPC synchronization shows the most resemblance to the swing equation and has the possibility of varying its behavior by changing the power loop parameters it is an interesting method to further analyse. The use of a virtual admittance structure is also an interesting concept that enables some flexibility in the control. The PSC- and droop method have in literature been proven to be suitable grid forming control methods but an in-depth study of these control methods are left for future work.

Chapter 4

Development of Simulation Models

The following chapter will introduce the studied system and the applied control method. The chapter will also describe how a Simulink model and a state space model were developed. The model referred to as the Simulink model is used for time domain simulations while the state space model is a linearized model, used for stability assessment simulations. The linearized model is linearized around a steady state operating point. The chapter is closed with a presentation of model validation results.

4.1 Simulink Model

As stated earlier on, the analysis will be focused on SPC-synchronization and comparisons will be made with a PLL controlled system. Thereby, the studied system will be much alike to that described in Chapter 3, but the system will be implemented in the rotating dq-frame instead of the $\alpha\beta$ -frame. Two simulink models have been established, one with SPC synchronization and one using a PLL. Otherwise the models are identical. The PLL-model will therefore describe a PLL-system with a voltage source behavior, inspired by [27].

With this setup of models it is possible to make comparisons between these synchronization methods and deeper investigate their differences. The modelled system will be described in detail in the following paragraphs. A graphical representation of the system overview is presented in Figure 4.1.

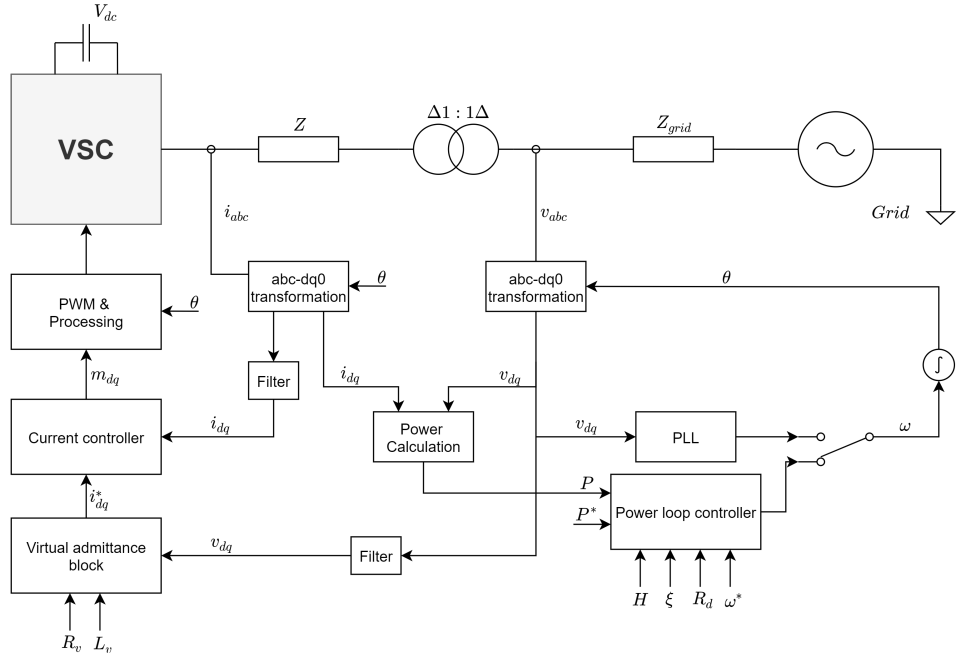


Figure 4.1: Graphical representation of the modelled system. In the figure it is illustrated that both SPC- and PLL synchronization can be applied to the system. In reality they are implemented as two different models.

The Simulink model is built by using the Simscape environment in Simulink. The voltage source converter is modeled as an average-value voltage source converter which is a building block in the Simscape environment, and it uses modulation signals from the PWM-generator to determine the switching behavior. The DC-side of the VSC is modelled as an ideal DC-voltage source. Hence, no restrictions are placed on the available active power reserve. This also implies that the DC-voltage at the converter terminal is kept constant and will therefore disregard any fluctuations in the DC-voltage when the energy storage system is loaded. As seen in Figure 4.1, the VSC is connected to a series impedance. The grid is then represented with a grid impedance in front of a three-phase voltage source. The short circuit power level of the grid can be varied in order to represent different grid strengths. It is also worth noting that the control system is implemented based on per unit quantities and that no reactive power control is implemented.

The Simulink model is solved using the automatic discrete time solver in Simulink, applied with a fixed time step of $5 \cdot 10^{-6}$ seconds. The PWM switching frequency is 5000 Hz, which corresponds to a time step of $2 \cdot 10^{-4}$ seconds. The following paragraphs will present details on the governing equations of the control system.

Synchronization

The system model incorporates both a PLL and the SPC-power loop controller. This allows for comparing simulations between the PLL- and SPC synchronization case. The PLL is implemented as,

$$\omega = \left(K_p^{PLL} + \frac{K_i^{PLL}}{s} \right) v_q \quad (4.1)$$

where K_p^{PLL} and K_i^{PLL} are proportional and integrating gains. The SPC-power loop controller is implemented as described in chapter 3,

$$\omega = \omega^* + \frac{K_p^{SPC}s + K_i^{SPC}}{s + K_g^{SPC}} (P^* - P) \quad (4.2)$$

where the parameters K_p^{SPC} , K_i^{SPC} and K_g^{SPC} can be set to govern the damping, inertia and droop

characteristics respectively, and can be derived to

$$\begin{aligned} K_i &= \frac{\omega_s}{2HS_N} \\ K_g &= \frac{1}{2HR_d} \\ K_p &= 2\xi\sqrt{\frac{\omega_s}{2HS_N P_{max}}} - \frac{1}{2HR_d P_{max}}. \end{aligned} \quad (4.3)$$

R_d is the slope of the droop-curve, ξ is the damping factor, S_N the nominal power of the generator and H is the inertia constant. Active power is calculated from the measured i_{dq} and v_{dq} components according to (2.23).

Voltage and Current Control

The virtual admittance block is implemented to provide a current reference to the current regulator. The admittance block should not be considered as a standard voltage controller but rather a means of providing a current reference, based on Ohm's law. The admittance structure provides the current reference in the following way:

$$\begin{bmatrix} \frac{di_d^*}{dt} \\ \frac{di_q^*}{dt} \end{bmatrix} = \frac{1}{L_v} \begin{bmatrix} -R_v & \omega L_v \\ -\omega L_v & -R_v \end{bmatrix} \begin{bmatrix} i_d \\ i_q \end{bmatrix} + \frac{1}{L_v} \begin{bmatrix} v_d^* - v_d \\ v_q^* - v_q \end{bmatrix}, \quad (4.4)$$

where R_v and L_v is the virtual resistance and inductance. The current controller is implemented as a standard PI-regulator with decoupling and a feed-forward term. The PWM-modulation signal is obtained using

$$\begin{aligned} m_d &= \frac{1}{V_{dc}/2} \left[(i_d^* - i_d) \left(K_p + \frac{K_i}{s} \right) + v_d - i_q L \omega \right] \\ m_q &= \frac{1}{V_{dc}/2} \left[(i_q^* - i_q) \left(K_p + \frac{K_i}{s} \right) + v_q + i_q L \omega \right], \end{aligned} \quad (4.5)$$

where the modulation signals are normalized by half the DC-voltage. The Simulink model also incorporates several filters.

4.2 State Space Model

The state space model is built on state space representations of each system component that are connected to form a multiple-input-multiple-output (MIMO) system representation. A graphical illustration of how the state space model is constructed is presented in Figure 4.2.

Each component is modelled either as an impedance or admittance structure. For example, the VSC is modelled as an admittance using the voltage difference between the secondary voltage and the modulation voltage as input and the converter currents as outputs. Modelling a component as an admittance gives the current as output signal while an impedance model gives the voltage as output. This is important for what states that will be observed in the over all system state space representation. The parameters of these admittances and impedances were set to match the Simulink model components. The control actions, such as the virtual admittance structure and the current controller, are modelled by rewriting the transfer function expressions as a state space representation and uses the same inputs and outputs as in the Simulink model.

In Figure 4.2 one can observe that control system is depicted to the left. The control system is then connected to interact with the synchronization representation. Similarly to the Simulink model is two versions of the state space model established, one where SPC-synchronization is applied and one where a PLL is implemented. The synchronization interaction is in the state space model represented as forward or backward rotation to the input signals depending on their direction. This is the same rotation that is applied in the $\alpha\beta$ to dq-transformation. After the rotation is applied some delays and sampling blocks are implemented in order match the behavior of the state space model with the Simulink one. Thereafter the VSC-model is connected to the STATCOM-circuit and network model. The converter current and

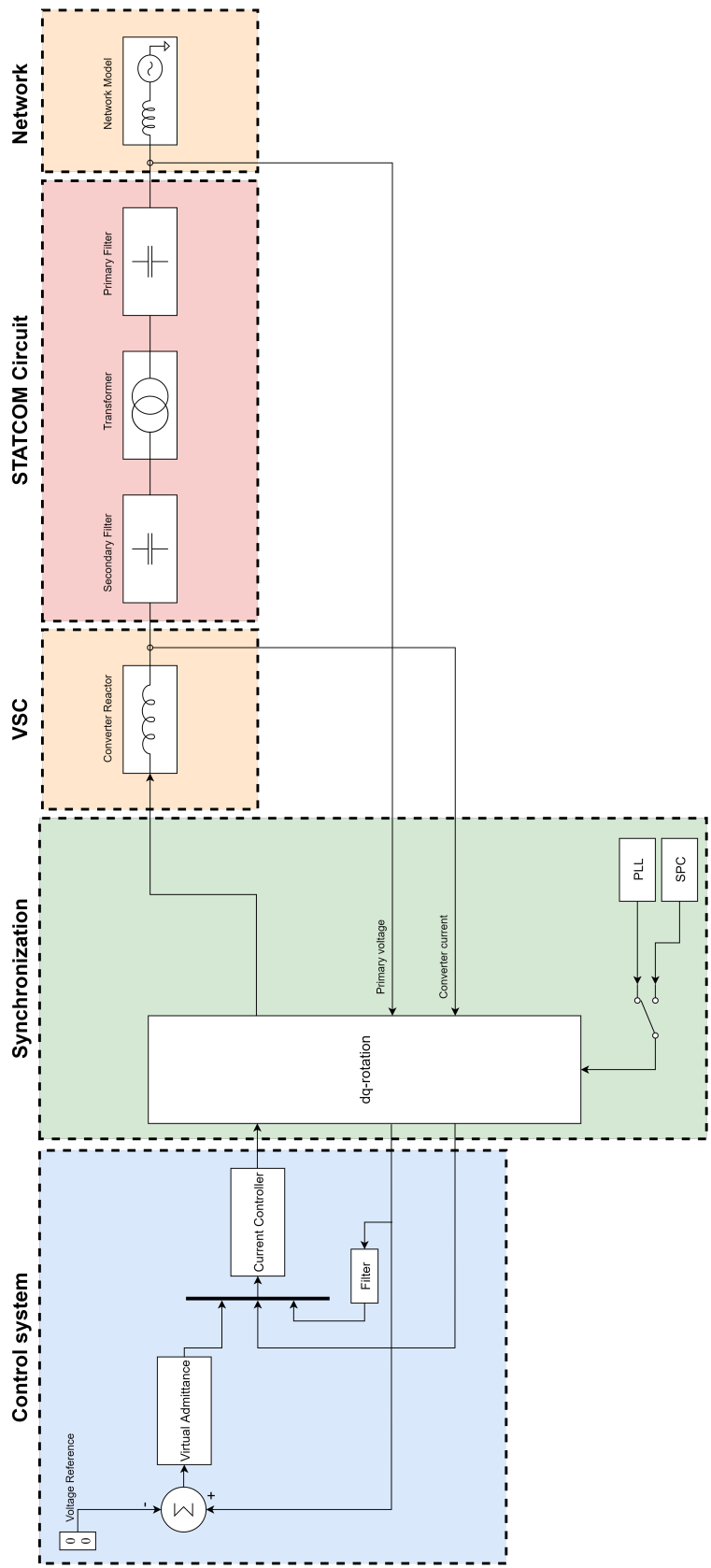


Figure 4.2: Simplified graphical representation of the developed state space model. Each system block is represented with a state space model.

PCC voltage is then fed back to the control system in order to close the loop. The process of creating a state space representation in dq-space is further described in Section 4.2.1.

In order to extract the system poles or simulate step responses, the system must be linearized. By applying the “Linear Analysis Tool” in the control system toolbox in Simulink a linearized model can be obtained. An input perturbation and output measurement are placed on the signals that the system is linearized around. The linearization points will not affect what poles that can be observed since they are common for the whole system, but the number of zeros will change depending on the linearization points. For model validation the input/output measurement is placed according to the comparing Simulink model signal. When the system is linearized the poles, zeros and pole-zero plots can be calculated.

4.2.1 Creation of State Space Representation in the dq-frame

The process of establishing a state space representation for a component in dq-space can be structured in the following way:

1. Each component (such as transformer, VSC, filters, etc...) is formulated as a transfer function described by an admittance or impedance. From the single line diagram in Figure 4.1, the transfer function $H(s)$ for a component is formulated as

$$Y(s) = H(s)X(s). \quad (4.6)$$

2. The transfer function is rewritten as a state space representation. Hence, from $H(s)$ the following state space representation is formulated:

$$\begin{aligned} \dot{x} &= Ax + Bu \\ y &= Cx + Du. \end{aligned} \quad (4.7)$$

3. The state space representation of the single line diagram should now be written in the $\alpha\beta$ -space. A single input system with n-states is explicitly written as:

$$\begin{aligned} \begin{bmatrix} x_1 \\ \vdots \\ x_n \end{bmatrix} &= \begin{bmatrix} a_{11} & \dots & a_{1n} \\ \vdots & \ddots & \vdots \\ a_{n1} & \dots & a_{nn} \end{bmatrix} \begin{bmatrix} x_1 \\ \vdots \\ x_n \end{bmatrix} + \begin{bmatrix} b_1 \\ \vdots \\ b_n \end{bmatrix} u_1 \\ y &= [c_1 \ \dots \ c_n] \begin{bmatrix} x_1 \\ \vdots \\ x_n \end{bmatrix} + \begin{bmatrix} d_1 \\ \vdots \\ d_n \end{bmatrix} u_1 \end{aligned} \quad (4.8)$$

If the system is balanced, the α and β -axis are identical. The state space model of the single line diagram can therefore be expanded and written as a state space representation in the $\alpha\beta$ -frame.

$$\begin{aligned} \begin{bmatrix} x_{\alpha 1} \\ x_{\beta 1} \\ \vdots \\ x_{\alpha n} \\ x_{\beta n} \end{bmatrix} &= \begin{bmatrix} a_{11} & 0 & \dots & a_{1n} & 0 \\ 0 & a_{11} & \dots & 0 & a_{1n} \\ \vdots & \vdots & \ddots & \vdots & \vdots \\ a_{n1} & 0 & \dots & a_{nn} & 0 \\ 0 & a_{n1} & \dots & 0 & a_{nn} \end{bmatrix} \begin{bmatrix} x_{\alpha 1} \\ x_{\beta 1} \\ \vdots \\ x_{\alpha n} \\ x_{\beta n} \end{bmatrix} + \begin{bmatrix} b_1 & 0 \\ 0 & b_1 \\ \vdots & \vdots \\ b_n & 0 \\ 0 & b_n \end{bmatrix} \begin{bmatrix} u_{\alpha 1} \\ u_{\beta 1} \\ \vdots \\ u_{\alpha n} \\ u_{\beta n} \end{bmatrix} \\ \begin{bmatrix} y_{\alpha 1} \\ y_{\beta 1} \end{bmatrix} &= \begin{bmatrix} c_1 & 0 & \dots & c_n & 0 \\ 0 & c_1 & \dots & 0 & c_n \end{bmatrix} \begin{bmatrix} x_{\alpha 1} \\ x_{\beta 1} \\ \vdots \\ x_{\alpha n} \\ x_{\beta n} \end{bmatrix} + \begin{bmatrix} d_1 & 0 \\ 0 & d_1 \\ \vdots & \vdots \\ d_n & 0 \\ 0 & d_n \end{bmatrix} \begin{bmatrix} u_{\alpha 1} \\ u_{\beta 1} \\ \vdots \\ u_{\alpha n} \\ u_{\beta n} \end{bmatrix} \end{aligned} \quad (4.9)$$

More compactly, this can be formulated as

$$\begin{aligned} \dot{x}_{\alpha\beta} &= A_{\alpha\beta}x_{\alpha\beta} + B_{\alpha\beta}u_{\alpha\beta} \\ y_{\alpha\beta} &= C_{\alpha\beta}x_{\alpha\beta} + D_{\alpha\beta}u_{\alpha\beta}. \end{aligned} \quad (4.10)$$

4. A representation of the system component is now obtained in the $\alpha\beta$ -frame. In order to transform the representation into the dq-space a rotation matrix Ω is applied to each $\alpha\beta$ -pair.

$$\Omega = \begin{bmatrix} \cos(\theta) & -\sin(\theta) \\ \sin(\theta) & \cos(\theta) \end{bmatrix} \quad (4.11)$$

This will introduce cross-coupling terms between each pair of dq-states. The cross-coupling matrix, R , can be defined as

$$R = \begin{bmatrix} 0 & \omega & 0 & 0 & \dots & \dots & 0 & 0 & 0 & 0 \\ \omega & 0 & 0 & 0 & \dots & \dots & 0 & 0 & 0 & 0 \\ 0 & 0 & \ddots & \ddots & \ddots & \ddots & \vdots & \vdots & \vdots & \vdots \\ 0 & 0 & \ddots & \ddots & \ddots & \ddots & \vdots & \vdots & \vdots & \vdots \\ \vdots & \vdots & 0 & 0 & \ddots & \ddots & 0 & 0 & \vdots & \vdots \\ \vdots & \vdots & 0 & 0 & \ddots & \ddots & 0 & 0 & \vdots & \vdots \\ \vdots & \vdots & \vdots & \vdots & \ddots & \ddots & \ddots & \ddots & 0 & 0 \\ \vdots & \vdots & \vdots & \vdots & \ddots & \ddots & \ddots & \ddots & 0 & 0 \\ 0 & 0 & 0 & 0 & \dots & \dots & 0 & 0 & 0 & \omega \\ 0 & 0 & 0 & 0 & \dots & \dots & 0 & 0 & \omega & 0 \end{bmatrix}, \quad (4.12)$$

which is a block diagonal matrix of cross coupling matrices $\begin{bmatrix} 0 & \omega \\ \omega & 0 \end{bmatrix}$ along the diagonal and zero matrices elsewhere. This enables the representation

$$\begin{aligned} \dot{x}_{dq} &= A_{dq}x_{dq} + B_{dq}u_{dq} \\ y_{dq} &= C_{dq}x_{dq} + D_{dq}u_{dq}. \end{aligned} \quad (4.13)$$

where

$$\begin{aligned} A_{dq} &= A_{\alpha\beta} - R \\ B_{dq} &= B_{\alpha\beta} \\ C_{dq} &= C_{\alpha\beta} \\ D_{dq} &= D_{\alpha\beta}. \end{aligned} \quad (4.14)$$

4.3 Model Validation

In order to confirm that the state space and Simulink model describe the same system behavior they must be validated against each other. In the following section the validation process will be presented for a system using both PLL and the SPC-synchronization. The state space representations of single building blocks have also been validated with their Simulink equivalent (where this is possible), the results from the validation is presented in Appendix C.

4.3.1 PLL-system

The validation procedure is performed using step response comparisons between the Simulink and state space model. Initially a step is placed on the current reference and investigates the validity of the current controller and circuit parameters. Thereafter a step is placed on the voltage reference. This encaptures the whole system dynamics and validates both the voltage and current controller as well as the synchronization and dq-transformations. Lastly an angle disturbance, in the form of a step of the voltage angle, is placed on the grid. This also validates the whole system dynamics and clearly shows if the PLL is able to regain synchronism after a disturbance.

Figure 4.3 shows the step response on current- (left) and voltage reference (right) for both the state space and Simulink model. A step of the grid angle of 5 degrees is also simulated and the v_q response is studied. For the PLL to regain synchronism the v_q voltage should go back to zero.

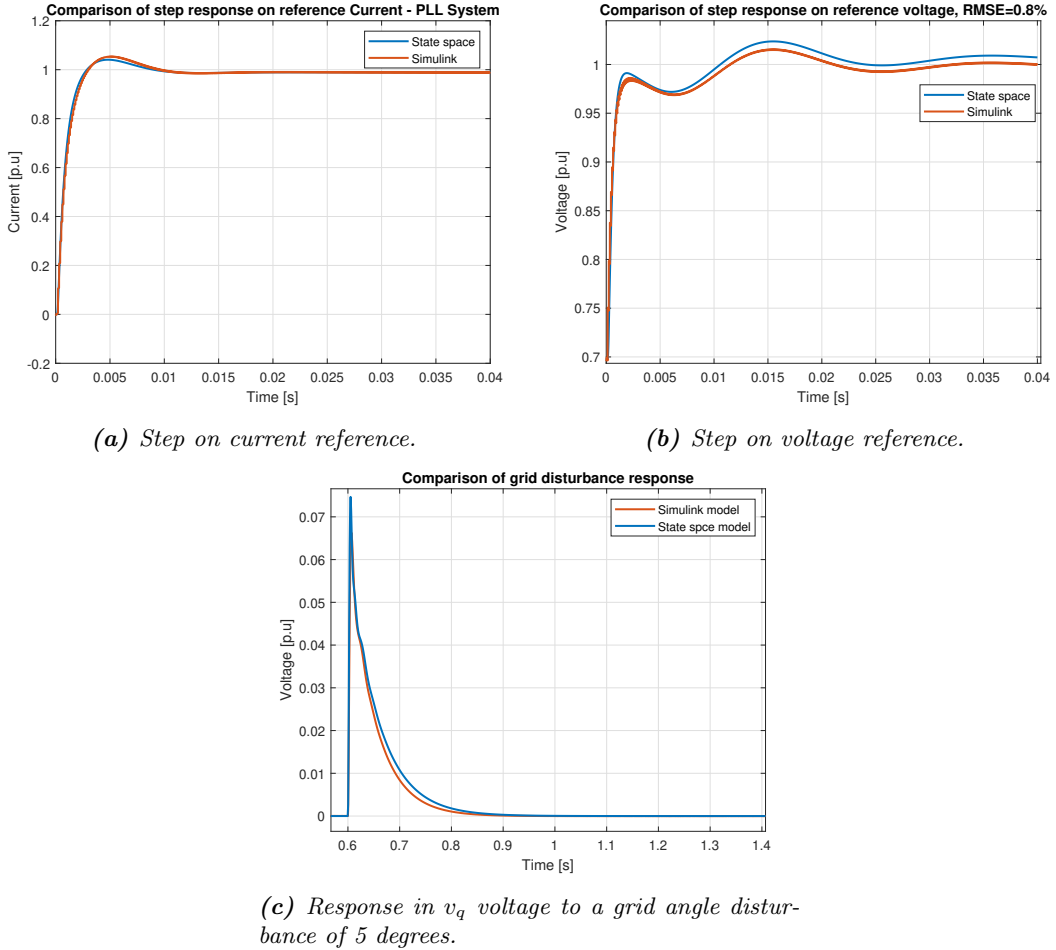
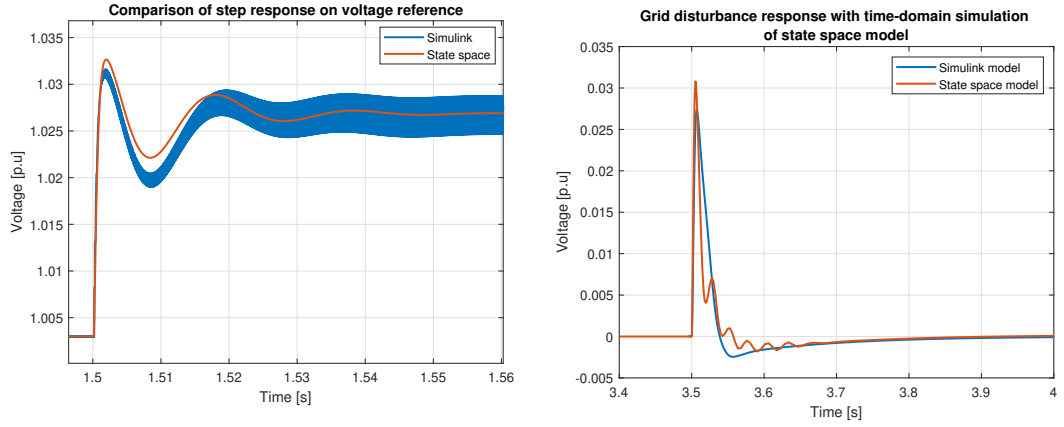


Figure 4.3: Validation of step response on current and voltage reference as well as grid disturbance response of v_q voltage. The Simulink system response is displayed in orange and state space response in blue.

Figure 4.3 shows that the responses are well matched and hence the models describe the same system dynamics. The PLL also operates as desired and is able to regain synchronism. The response of the PLL-system however is rather slow and this is a result of how the PLL PI-controller was tuned. A small difference can be seen in the simulation of a step change on the reference voltage. It can however be noted that the system behavior is much alike, but a steady state error can be observed. The root mean square error between the responses can be calculated to 0.8 %. This small error, together with the well matched responses in Figure 4.3, proves that the two models largely describe the same system dynamics.

4.3.2 SPC-system

The two models are also validated using the SPC-synchronization method. In Figure 4.4, the results of a step on the voltage reference as well as a step on the grid angle is presented.



(a) Step on voltage reference for the SPC-system.
The noise in the Simulink signal is due to the use
of an unfiltered voltage signal.

(b) Response in v_q voltage to a grid angle disturbance.

Figure 4.4: Validation of step response on voltage reference as well as grid disturbance response of v_q voltage using SPC-synchronization.

Figure 4.4 shows that there is not a perfect match between the two models. The same system behavior can be noted even though there are some mismatches in the responses. Specifically, an oscillatory behavior can be noted on the grid disturbance response. It can be noted that the there is no steady state error between the models and the oscillatory behavior in the state space model could be solved by implementing a low pass filter.

In summary, one can note that the simulink and state space model seems to capture the same characteristics both in the PLL and SPC-system even though some mismatches are noted. These mismatches are not major and some discrepancies is expected since these are complex models. Therefore, by the results presented in Figure 4.3 and 4.4 the two models is to be considered as validated.

Chapter 5

Simulation Results

In this chapter the performance of the SPC- method will be evaluated using both continuous time and linearized model simulations. Comparisons will be made with a system where the synchronization method has been replaced with a PLL and will thus compare a grid forming and grid following synchronization method.

5.1 Continuous Time Simulations

This section seeks to investigate the performance of the SPC control method by the means of continuous time simulations, made possible by the Simulink model. Both the frequency and voltage behavior will be studied in detail and comparisons will be made with a grid following system. Initially the frequency behavior is analysed.

5.1.1 Frequency Behavior

To validate that the SPC system is functioning desirably, a step on the power reference is executed. The result is presented in Figure 5.1.

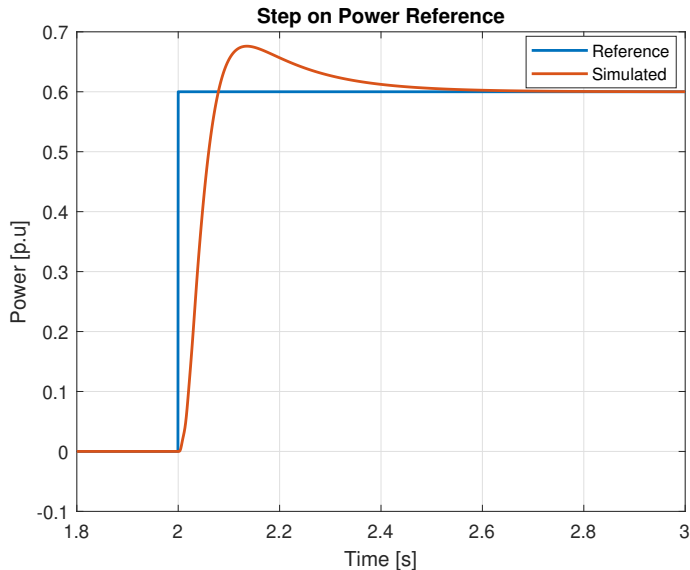


Figure 5.1: Step response of the active power.

From Figure 5.1 one can observe that the control signal reaches the reference value without steady-state

error. The response is however relatively slow and has some overshoot. It is though expected that the SPC would respond relatively slow due to the inertia factor in the power-loop equation, the response is simulated with the inertia factor, $H = 5$.

In Figure 5.2 a change of the grid frequency and the sequent active power response is displayed.

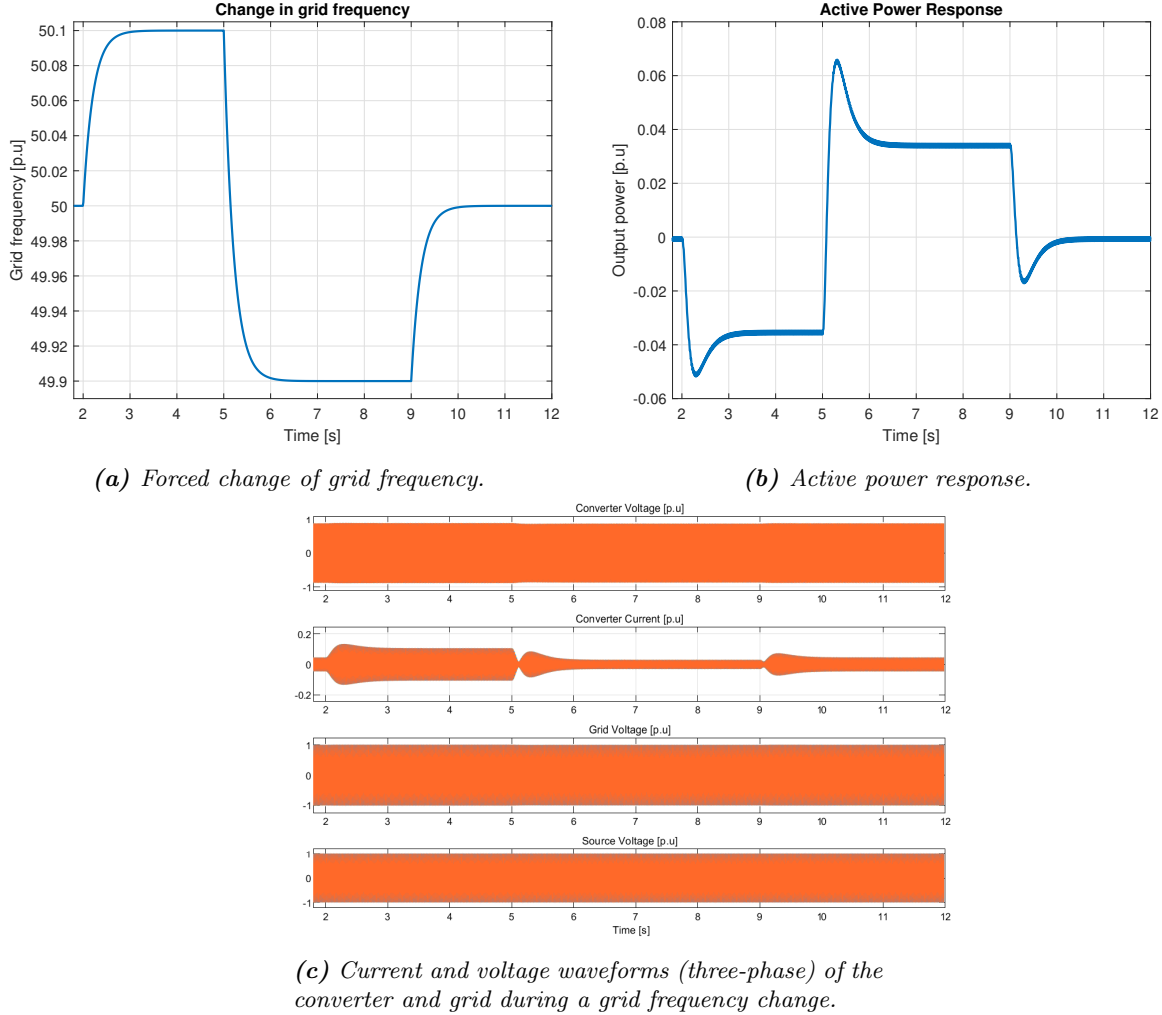
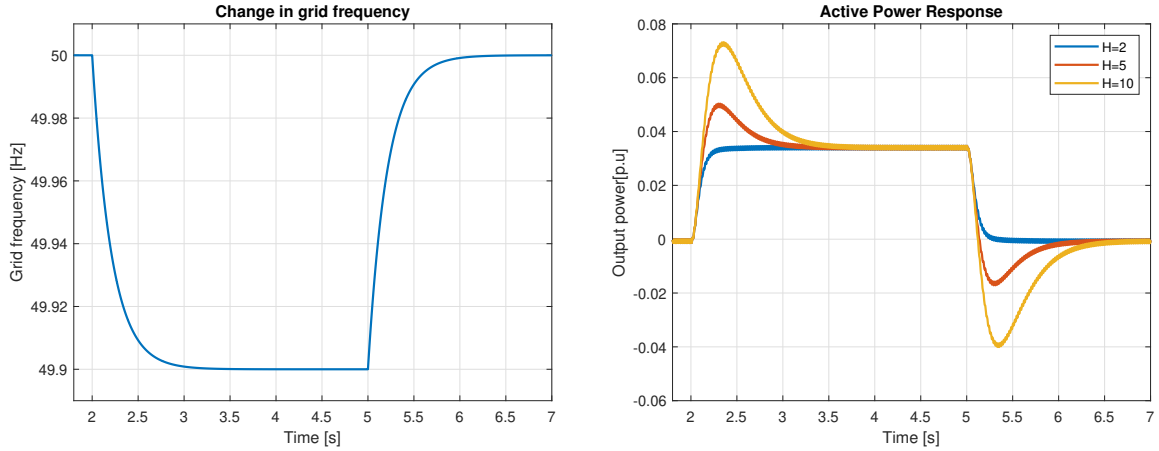


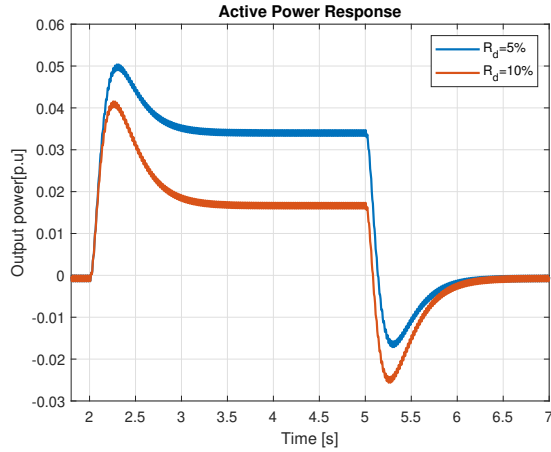
Figure 5.2: Active power response to grid frequency changes.

Figure 5.2 shows that the SPC incorporates a similar behavior to a synchronous machine that provides frequency regulation. When the frequency on the grid goes above 50 Hz, the grid frequency is too large and the converter tries to “take” power from the grid in order to slow it down. When the grid frequency goes below 50 Hz the grid is instead below the desired frequency and the converter injects power in order to compensate. By studying the converter voltage and current waveforms one can observe that the power injection is governed by the current magnitude.

A further investigation on how the different SPC-parameters affect the active power response is conducted in Figure 5.3.



(a) The grid frequency is forced to 49.9 Hz and then (b) Active power response for different inertia constants.
 (c) Active power response with different R_d values.



(c) Active power response with different R_d values.

Figure 5.3: Active power response to grid frequency changes with variations in inertia constant and droop slope. Remember that R_d describes the frequency deviation in percent that results in a change of power by the value of S_N .

In Figure 5.3 it can be noted that the converter can operate in a stable manner for different inertia constants. It can also be observed that larger inertia constants enables a larger active power response where more power is transferred in order to withstand the frequency change. Power is also exchanged for a longer period, as indicated by the swing equation that were introduced in Chapter 2. The droop slope parameter, R_d , changes where the plateau of the active power response occurs and a steeper slope can be observed as a lower plateau.

5.1.1.1 Comparison Between SPC and Grid Following PLL

Figure 5.4 shows a comparison of the active and reactive power response due to a disturbance of the grid voltage angle. The comparison is made between the SPC-method and the PLL-system, where the PLL-system has been adjusted to behave in a grid following way. The angle jump will force the synchronization-loop to regain synchronism with the grid and the active and reactive power response can be studied to gain insight in how the synchronization is restored.

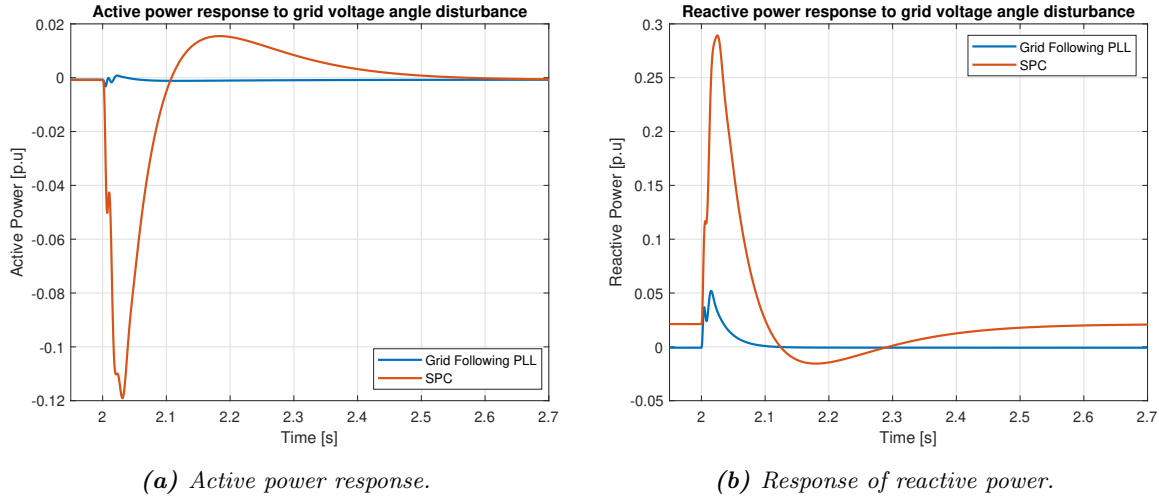


Figure 5.4: Response of active and reactive power to a grid voltage angle disturbance of 5 degrees. The disturbance is introduced after 2 seconds.

Figure 5.4 shows that the resynchronization using the SPC-method is associated with a transfer of power. This illustrates that the converter actually behaves like a synchronous machine would. In the grid following case, no major power transfer is present. This is due to the fact that the synchronization is not based on the principles of power transfer but rather on regulating the v_q -voltage to zero. Note that no control of the reactive power is implemented in the SPC-case. It is therefore possible that the reactive power has a nonzero steady state value.

5.1.2 Voltage Behavior

In this section, the voltage behavior of the SPC-system is investigated. Figure 5.5 presents PCC and grid voltage magnitude response to a disturbance where the grid voltage magnitude is stepped to 1.05 p.u. The grid disturbance is simulated for the SPC-system but also for a grid following system where no voltage controller is implemented and the synchronization is provided by a PLL. The figure also shows the response for a PLL-system with a voltage controller.

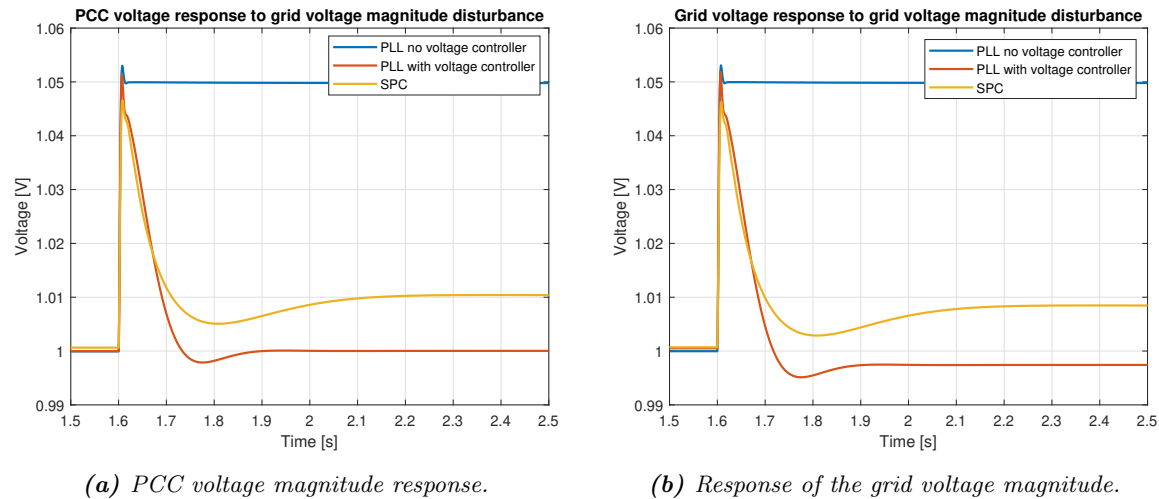


Figure 5.5: PCC and grid voltage responses to a disturbance of 1.05 p.u. in the grid voltage magnitude, placed at 1.6 seconds.

The SPC-system is able to handle the disturbance and regress close to the value before the disturbance.

The same is true for the case where a voltage regulator is implemented. It can however be noted that the voltage controller makes the voltage go back to the reference value whereas the SPC-system displays an offset compared to the steady state value before the disturbance. This is due to the fact that the virtual admittance structure does not regulate voltage in the same sense as the voltage controller does. The voltage controller reacts to push the signal to its reference value since it is a PI-regulator. The virtual admittance structure is not a regulator in the same sense. The voltage reference value in the admittance structure is used to calculate the reference current. It is therefore possible that there will be an offset between the reference and the output. However, a voltage forming behavior is noted.

The grid following PLL, where no voltage controller is implemented, is not able to actively control its voltage output and thus the voltage magnitude will follow the grid voltage magnitude.

5.2 Stability Assessment and Identification of Poles

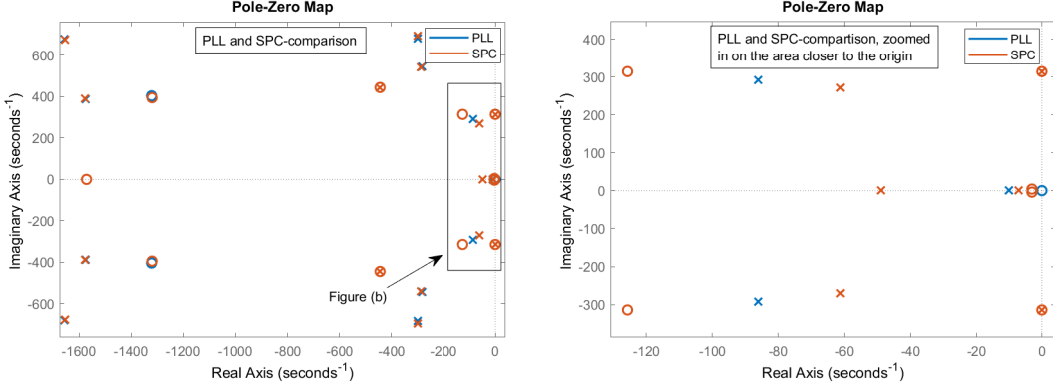
In order to further investigate what it means to switch from a grid following to a grid forming control the location of poles and zeros will be analyzed. Comparisons will be made between a PLL-system, implementing a voltage forming behavior (the virtual admittance), here denoted as the “GFM-PLL-System”, and the SPC-system, denoted “GFM-SPC”. This makes it possible to compare a grid-forming and a grid-following synchronization method. A comparison will also be made with a grid-following PLL-system denoted as “GFL-PLL”. If the PLL and the SPC model are linearized with a PCC voltage angle disturbance as input and the PCC voltage magnitude as the output, the system poles and zeros can be studied. All system poles and zeros are presented in Table A.1, found in Appendix A.

In the Appendix and Table A.1 it can be seen that there are no right-half-plane poles, indicating that the PLL and SPC systems are stable. There are also several poles that are canceled by equivalent zeros and it could be concluded that some poles are not of particular interest. The poles that need further investigation is presented in Table 5.1. The table also presents the natural frequencies, ω_n , and damping factors, ξ , of the poles.

Table 5.1: Comparison of poles for the PLL and SPC system. Matching poles are marked in green, unmatched poles in red and close to matching poles in yellow. Poles canceled by equivalent zeros are not displayed.

Nr.	GFM-PLL			GFM-SPC		
	Pole	ω_n	ξ	Pole	ω_n	ξ
1.	-4.7703+2.0276e+08i	2.0276e+08	2.35e-08	-4.7703+2.0276e+08i	2.0276e+08	2.35e-08
2.	-4.7703-2.0276e+08i	2.0276e+08	2.35e-08	-4.7703-2.0276e+08i	2.0276e+08	2.35e-08
3.	-4.7703+2.0276e+08i	2.0276e+08	2.35e-08	-4.7703+2.0276e+08i	2.0276e+08	2.35e-08
4.	-4.7703-2.0276e+08i	2.0276e+08	2.35e-08	-4.7703-2.0276e+08i	2.0276e+08	2.35e-08
15.	-1654.7+678.74i	1788	0.92	-1654+676.48i	1788	0.92
16.	-1654.7-678.74i	1788	0.92	-1654-676.48i	1788	0.92
17.	-1574.5+388.74i	1621	0.97	-1576+389.09i	1623	0.97
18.	-1574.5-388.74i	1621	0.97	-1576-389.09i	1623	0.97
19.	-300.97+682.69i	746.1	0.40	-299.15+693.97i	755.7	0.40
20.	-300.97-682.69i	746.1	0.40	-299.15-693.97i	755.7	0.40
21.	-283.59+544.2i	613.7	0.46	-287.53+540.99i	612.66	0.47
22.	-283.59-544.2i	613.7	0.46	-287.53-540.99i	612.66	0.47
23.	-9.862+0i	9.862	1	-6.9082+0i	6.908	1
24.	-85.958+291.52i	303.9	0.28	-48.903+0i	48.90	1
25.	-85.958-291.52i	303.9	0.28	-61.207+271i	277.8	0.22
36./26.	-18850+0i	18850	1	-61.207-271i	277.8	0.22
37./39.	-18850+0i	18850	1	-18850+0i	18850	1
-/40.				-18850+0i	18850	1

Several of the poles between the PLL and SPC-system match or are close to match, as can be seen in Table 5.1. This is however expected since the systems only have different synchronization mechanisms. But, six poles do not match and are affected by the synchronization. A graphical representation of the different pole-zero locations is given in Figure 5.6.



(a) Pole-zero plot comparison zoomed in on the (b) Further zoomed in pole-zero plot on the area area where a mismatch in pole location is noticed. around the origin.

Figure 5.6: Pole-zero plots of the PLL-system (blue) and SPC-system (orange). Poles are marked with X and zeros with O. Some poles and zeros presented in Table A.1 are not displayed.

5.2.1 Influence of the Virtual Admittance

This section investigates how the virtual admittance structure influence the pole locations. In Table 5.2 the poles that are affected by the impedance change are marked.

Table 5.2: Poles that are affected by a change of the virtual impedance are marked in green. Small changes is marked in light green and larger changes marked with a darker green.

Nr.	GFM-PLL Poles	GFM-SPC Poles
15.	-1654.7+678.74i	-1654+676.48i
16.	-1654.7-678.74i	-1654-676.48i
17.	-1574.5+388.74i	-1576+389.09i
18.	-1574.5-388.74i	-1576-389.09i
19.	-300.97+682.69i	-299.15+693.97i
20.	-300.97-682.69i	-299.15-693.97i
21.	-283.59+544.2i	-287.53+540.99i
22.	-283.59-544.2i	-287.53-540.99i
23.	-9.862+0i	-6.9082+0i
24.	-85.958+291.52i	-48.903+0i
25.	-85.958-291.52i	-61.207+271i
-/26.		-61.207-271i

Comparing Table 5.1 and 5.2 clarifies that the same poles are affected by a change in virtual impedance as a change of synchronization method. This indicates that the red coloured poles in Table 5.1 and dark green coloured poles in 5.2 are the ones that are most coupled to the synchronization method and the voltage/current control. But there poles colored in yellow and light green also seem to show a connection.

It is also interesting to note how this change of the virtual impedance changes the system behavior. Figure 5.7 displays how the SPC-pole at $-61.2 \pm 271i$ changes as the resistance and inductance is varied.

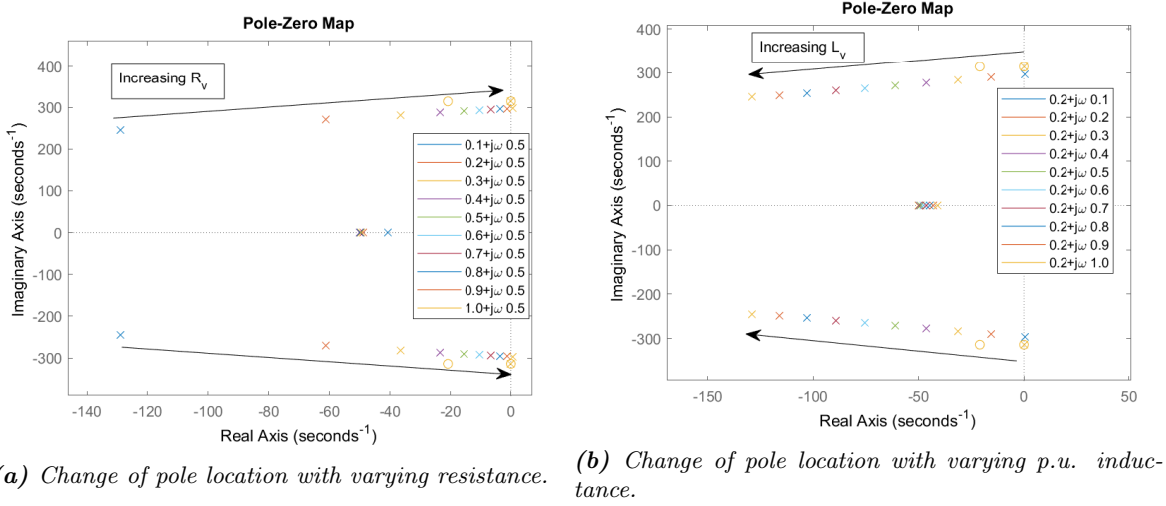


Figure 5.7: The figure displays how the SPC-pole at $-61.2 \pm 271i$ changes as the virtual resistance and inductance is varied. The impedance values are given in p.u.

From Figure 5.7 it can be observed that increasing the virtual resistance of the impedance will make the system respond slower and also eventually push it over the stability limit. The system will not only respond slower but also be less damped. The contrary is true for an increase of the virtual inductance, where an improved behavior is noticed both in terms of speed and damping. It can be concluded that the virtual admittance introduces the possibility of ensuring a high X/R-ratio so that the assumptions for (3.11) is valid. The above presented results proves that a high X/R-ratio seems beneficial. It is worth noting that these simulations were carried out in a strong grid environment.

5.2.2 Participation Factors

To further investigate from which system components different poles originate, the tool of participation factors is applied. Participation factors provides a measure of the participation between state variables and poles, as stated in chapter 2. The investigation is performed on the SPC-system but is also applicable on the PLL system since the underlying system is the same.

The state space model consist of 40 states in total and a description of their represented parts in the state space model is displayed in Table 5.3. Note that it requires two states to capture both the d- and q-component and that some system components may have more than two inputs, hence several states is required for one state space representation of such a system component.

Table 5.3: States used in the state space model and their represented part of the model.

Nr.	Description	Nr.	Description
1.	Converter reactor	21.	Filter on grid voltage
2.	Converter reactor	22.	Filter on grid voltage
3.	Feed-forward (FF) filter	23.	Network model
4.	FF-filter	24.	Network model
5.	Primary STATCOM filter	25.	SPC model
6.	Primary STATCOM filter	26.	SPC model
7.	Secondary STATCOM filter	27.	Virtual admittance model
8.	Secondary STATCOM filter	28.	Virtual admittance model
9.	Current controller output	29.	Filter on input to FF-filter
10.	Current controller output	30.	Filter on input to FF-filter
11.	Current controller output	31.	Filter on input to FF-filter
12.	Current controller output	32.	Filter on input to FF-filter
13.	Current controller output after delays	33.	Filter on grid voltage to virt. adm.
14.	Current controller output after delays	34.	Filter on grid voltage to virt. adm.
15.	Filter on converter current	35.	Filter on grid voltage to virt. adm.
16.	Filter on converter current	36.	Filter on grid voltage to virt. adm.
17.	Filter on voltage to FF-part	37.	Transformer
18.	Filter on voltage to FF-part	38.	Transformer
19.	Filter on converter current	39.	Transformer
20.	Filter on converter current	40.	Transformer

By calculating the participation factors for the linearized model, a 40×40 matrix is produced. A matrix element PF_{ki} is a measure of the participation of the k th state in the i th mode. These participation factors are presented in a three dimensional plot in Figure 5.8.

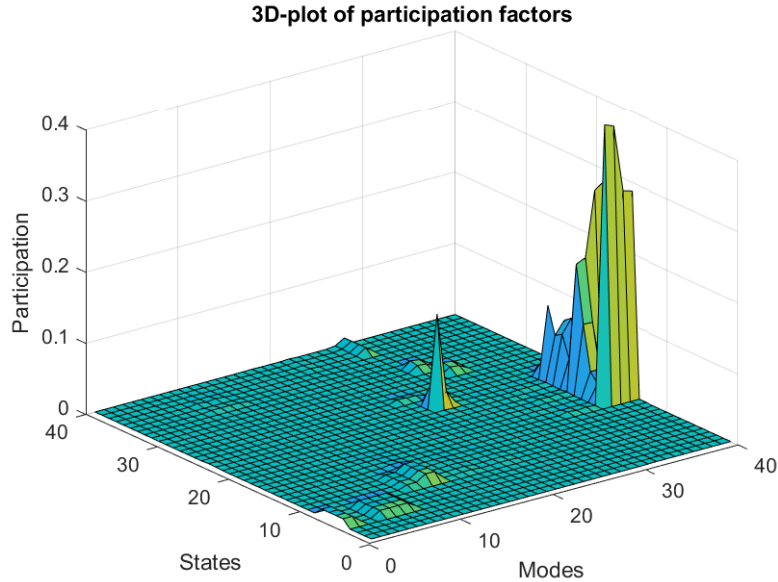


Figure 5.8: Illustration of participation factors where the participation between different states and modes can be observed.

From Figure 5.8 it can be observed that most of the states and modes show low participation. The largest participation factors are found for modes related to poles that by previous investigation was concluded

to not be of interest.

By studying the factors closer it can also be concluded that states 5-8 are linked as well as states 9-12, since they show the same participation factors. The same goes for state 37-40. This is expected since state 5-8 describes the filters used in the STATCOM-circuit. State 9-12 describes the output of the current controller and states 37-40 models the transformer, all according to Table 5.3. It is therefore expected that these states are connected and the fact that this can be observed in the participation factors gives authority to the results.

Even though the participation factors for the interesting poles, illustrated in red and yellow in Table 5.1, are small they can be analyzed for further insights. In Figure 5.9 and 5.10 the participation factors for poles 15-26 are presented.

The results presented in Figure 5.9 and 5.10 are summarized below. Note that pole 23 and 24 are the ones located closest to the imaginary axis and hence of most concern for stability reasons.

- Figure 5.9 illustrates that pole 15-18 are mostly coupled to the 9-12th states that describe the current controller output.
- Pole 19 shows largest participation in the 24th and 23rd state, that corresponds to the network model of the system.
- Pole 20 shows large participation in the state describing the filter applied on the primary grid voltage. Hence it is also connected to the grid and network behavior. Pole 20 also show some participation in the SPC-state as well as in the states regarding the filter applied on the controller output.
- The participation of pole 21 mainly involves the states of the current controller output (states 9-12). Pole 22 also shows large participation in these states but shows even larger participation in states 37-40, related to the transformer.
- The participation plot clearly indicates that poles 23 and 24 only show participation with state 26 that relates to the SPC-synchronization.
- Figure 5.10 shows that the participation factors are close to zero except for state 23 for both pole 25 and 26. This indicates that these poles are mostly related to the network model (state 23 & 24).
- It is worth noting that the participation factors are small for the aforementioned poles but still provides an indication on the relative participation.

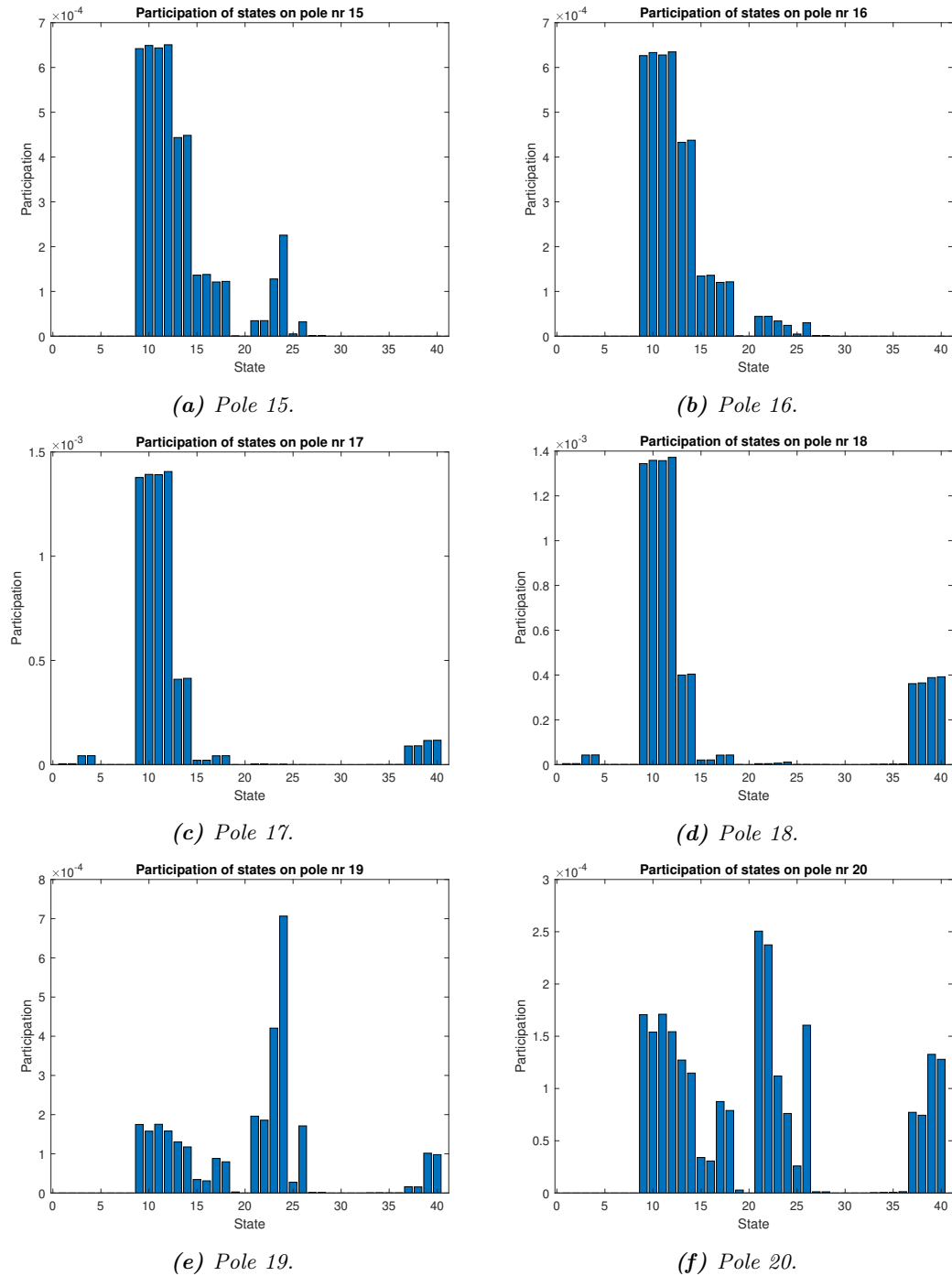


Figure 5.9: Participation factors for pole 15-20 on the different states.

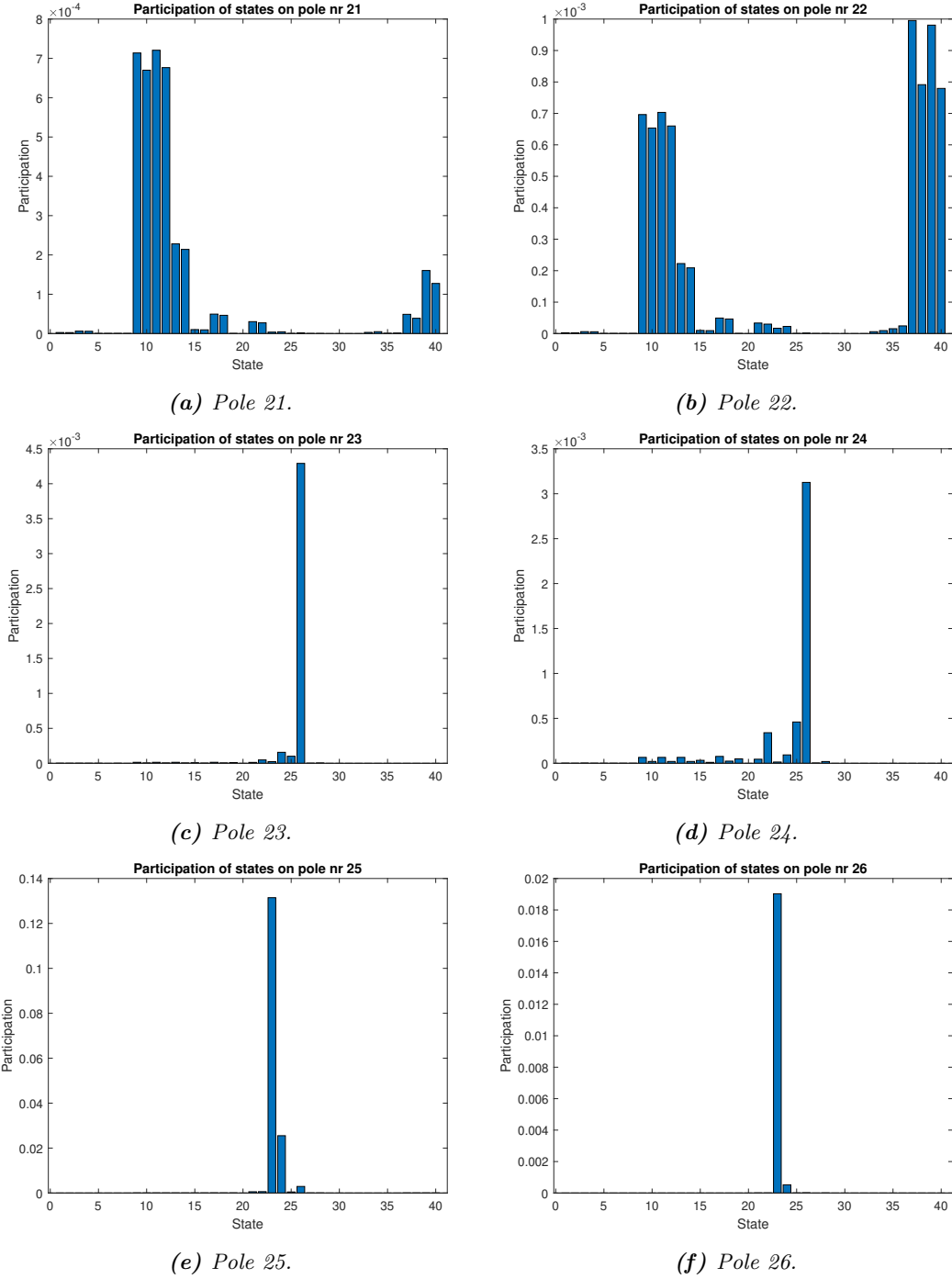


Figure 5.10: Participation factors for pole 21-26 on different model states.

5.2.3 Comparison of Pole Locations With a Grid Following PLL-System

This section seeks to compare the pole locations of the previously analysed SPC- and PLL-system with a grid following PLL-system, here denoted as GFL-PLL. Remember that the only component differentiating the SPC-and PLL-system is the synchronization, where the SPC-system utilizes a power-synchronization loop and the PLL-system uses a PLL. But, the voltage behavior is the same since the virtual admittance structure is implemented in both systems. Comparisons will here be made with a grid following system, thus both voltage and frequency following. The comparison will also present the natural frequencies, ω_n , and damping factors, ξ , of the poles as seen in Table 5.4.

Table 5.4: The table presents a comparison of the most relevant pole locations between the GFM-SPC- and GFM-PLL-system but also with a grid following PLL system, here denoted GFL-PLL. The table also presents the natural frequency, in rad/s, and damping factor for the poles. The poles are sorted based on the natural frequency, the numbering used in previous tables does not apply in this table.

GFM-SPC			GFM-PLL			GFL-PLL		
Pole	ω_n	ξ	Pole	ω_n	ξ	Pole	ω_n	ξ
-6.9082+0i	6.908	1.00	-9.862+0i	9.862	1.00	-14.578+0i	14.58	1.00
-48.903+0i	48.90	1.00	-85.958+291.52i	303.9	0.28	-309.67+377.6i	488.3	0.63
-61.207+271i	277.8	0.22	-85.958-291.52i	303.9	0.28	-309.67-377.6i	488.3	0.63
-61.207-271i	277.8	0.22	-283.59+544.2i	613.7	0.46	-365.66+491.87i	612.9	0.60
-287.53+540.99i	612.6	0.46	-283.59-544.2i	613.7	0.46	-365.66-491.87i	612.9	0.60
-287.53-540.99i	612.6	0.46	-300.97+682.69i	746.1	0.40	-1526.2+437.98i	1587	0.96
-299.15+693.97i	755.7	0.40	-300.97-682.69i	746.1	0.40	-1526.2-437.98i	1587	0.96
-299.15-693.97i	755.7	0.40	-1574.5+388.74i	1621	0.97	-1562.5+726.91i	1723	0.91
-1576+389.09i	1623	0.97	-1574.5-388.74i	1621	0.97	-1562.5-726.91i	1723	0.91
-1576-389.09i	1623	0.97	-1654.7+678.74i	1788	0.93			
-1654+676.48i	1787	0.93	-1654.7-678.74i	1788	0.93			
-1654-676.48i	1787	0.93						

In Table 5.4 it can be seen that the SPC- and PLL-system shows similar behavior, especially for frequencies above 600 rad/s where the damping behavior and introduced frequencies are almost identical. A difference can however be noted for the lower frequencies. These poles are placed on the real axis and hence the damping factor is one. The participation factors indicated that these poles relates to the synchronization. The SPC-poles are placed closer to the origin than the PLL-poles, indicating a slower response in the SPC-case. It can also be noted that the SPC-system is slightly less damped in frequencies around 300 rad/s compared to the PLL-system.

For the grid following PLL one can observe that it displays fewer poles then the SPC- and PLL-system due to the fact that no voltage control is implemented. The pole with lowest natural frequency is placed further away from the origin than in the SPC and PLL case, indicating a faster response. The grid following system also seem to show better damping behavior in the frequency range of 400-600 rad/s but slightly less damping for frequencies above 1500 rad/s compared to the SPC- and PLL-system. The improved damping for the grid following PLL in the range of 400-600 rad/s could be a result of that no voltage control is implemented and hence less control actions is performed. The improved damping of the SPC and GFM-PLL for higher frequencies could be due to the voltage source behavior.

It was previously concluded that the GFM-PLL system has a faster response than the SPC-system. However, the SPC response can be adjusted by varying the parameters in the power synchronization loop. Here the SPC-system is adjusted in order to see if it is possible to adjust the SPC-parameters in such a way that the SPC poles are similarly placed as the GFM-PLL poles. Table 5.5 shows the pole locations for an adjusted SPC-system.

Table 5.5: Comparison between an adjusted SPC system where the SPC-parameters have been modified to match the GFM-PLL pole locations as close as possible.

Adjusted GFM-SPC			GFM-PLL		
Pole	ω_n	ξ	Pole	ω_n	ξ
-10.74+2.6586i	11.06	0.97	-9.862+0i	9.862	1.00
-10.74-2.6586i	11.06	0.97	-85.958+291.52i	303.9	0.28
-77.504+282.51i	293.0	0.26	-85.958-291.52i	303.9	0.28
-77.504-282.51i	293.0	0.26	-283.59+544.2i	613.7	0.46
-286.74+543.38i	614.4	0.47	-283.59-544.2i	613.7	0.46
-286.74-543.38i	614.4	0.47	-300.97+682.69i	746.1	0.40
-301.15+687.83i	750.9	0.40	-300.97-682.69i	746.1	0.40
-301.15-687.83i	750.9	0.40	-1574.5+388.74i	1621	0.97
-1575.1+388.8i	1622	0.97	-1574.5-388.74i	1621	0.97
-1575-388.8i	1622	0.97	-1654.7+678.74i	1788	0.93
-1654+676.48i	1787	0.93	-1654.7-678.74i	1788	0.93
-1654-676.48i	1787	0.93			

Table 5.5 illustrates that it is possible to adjust the SPC-parameters so that the SPC pole locations are close to match the PLL poles. The original SPC-parameters and the adjusted ones are presented in Table 5.6.

Table 5.6: Original SPC-parameters and adjusted parameters in order to match the GFM-PLL poles.

Parameter	Original	Adjusted
H	5	12.5
ξ	0.7	0.58
R_d	0.05	0.02

From Table 5.6 it can be observed that an increase of the inertia constant and a reduced damping factor is needed in order to match the pole locations. Table 5.5 indicates that a grid-forming and a grid-following synchronization method actually can display the same behavior.

5.2.4 Grid Strength Impact on Pole Locations

In this section it is investigated whether the grid strength affect the pole locations. The grid strength is defined in terms of Short Circuit Ratio (SCR) where $SCR \geq 5$ defines a strong grid, $5 > SCR > 3$ a moderate grid and $SCR \leq 3$ a weak grid. It is possible to change the SCR by adjusting the network impedance in the simulation models. One should note that a weak grid hereafter will be considered as a grid with low grid strength but still has high inertia since the inertia of the network model is unchanged.

GFM-SPC-system

The results for the SPC-system are presented in Table 5.7 and Figure 5.11. Note that only pole 15-26 (with the numbering introduced in Table A.1 and 5.1) are displayed in Table 5.7.

Table 5.7: Pole locations for different grid strengths (defined in terms of short circuit ratio). The investigation is performed on the **GFM-SPC-system**.

Nr	SCR=20	SCR=5	SCR=3	SCR=2
15.	-1654+676.48i	-1484.1+661.5i	-1458.2+651.81i	-1445.2+645.99i
16.	-1654-676.48i	-1484.1-661.5i	-1458.2-651.81i	-1445.2-645.99i
17.	-1576+389.09i	-1446.9+499.01i	-1418.4+512.56i	-1402.9+518.74i
18.	-1576-389.09i	-1446.9-499.01i	-1418.4-512.56i	-1402.9-518.74i
19.	-299.15+693.97i	-81.413+790.12i	-6.5869+794.46i	41.043+791.77i
20.	-299.15-693.97i	-81.413-790.12i	-6.5869-794.46i	41.043-791.77i
21.	-287.53+540.99i	-121.45+580.69i	-70.846+579.36i	-39.818+575.31i
22.	-287.53-540.99i	-121.45-580.69i	-70.846-579.36i	-39.818-575.31i
23.	-6.9082+0i	-8.2926+0i	-9.7335+3.7447i	-7.2944+5.0094i
24.	-48.903+0i	-19.105+0i	-9.7335-3.7447i	-7.2944-5.0094i
25.	-61.207+271i	-36.547+289.06i	-30.536+295.99i	-27.252+300.69i
26.	-61.207-271i	-36.547-289.06i	-30.536-295.99i	-27.252-300.69i

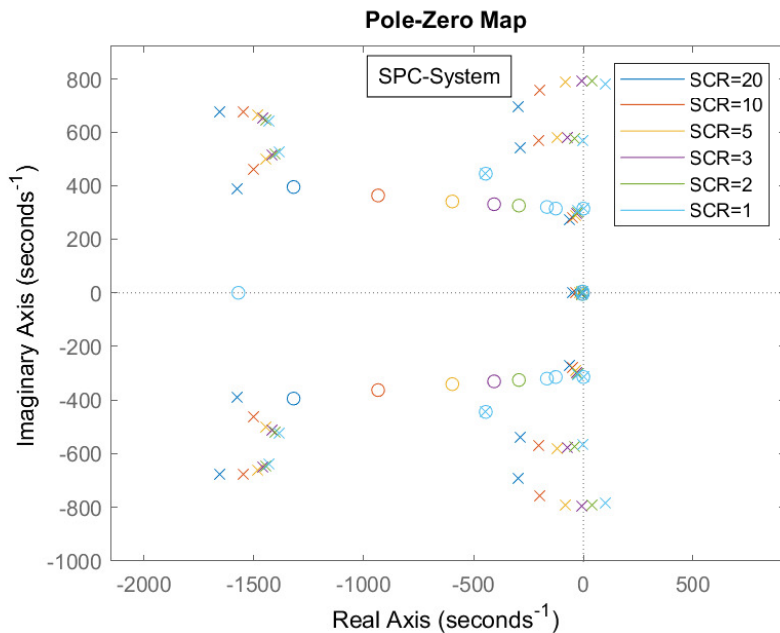


Figure 5.11: The figure shows a graphical representation of Table 5.7, zoomed in on the poles closest to the origin.

It can be observed that for SCR=2 one pole pair goes into the right half plane, indicating an unstable system. It can also be noted that as the grid strength is reduced, most of the poles shifts towards the right. This shift moves pole number 19 and 20 over the imaginary axis to the positive halfplane. This overall shift of poles to the right indicates that the system response will be slower and that the system is pushed closer to the stability limit. The dominating trend is also a growing imaginary part of the poles, meaning that the system becomes less damped for lower SCRs. This goes together with the system being pushed closer to the stability limit.

However, it is only one pole pair that has moved to the right halfplane, all other poles are still located in the left halfplane. Pole 19 and 20 were previously identified as that they had some connection with the control system but did not display large changes as the values of the virtual impedance were altered, or when the control method was changed from PLL to SPC. It could be the case that it is not the

SPC-system itself that goes unstable but rather poles describing some other parameter. Therefore it could be interesting to also investigate the GFM-PLL case.

GFM-PLL-system

Now, the shift of pole locations for the same variation of grid strength as before is investigated for the PLL-case. The results are presented in Table 5.8 and Figure 5.12. Table 5.8 however only displays pole number 15-25. The numbering is consistent with the numbering used in Table 5.7.

Table 5.8: Pole locations for different grid strengths now on the **GFM-PLL-system**.

Nr	SCR=20	SCR=5	SCR=3	SCR=2
15.	-1654.7+678.74i	-1483.9+661.97i	-1458+652.06i	-1445+646.15i
16.	-1654.7-678.74i	-1483.9-661.97i	-1458-652.06i	-1445-646.15i
17.	-1574.5+388.74i	-1446.7+498.86i	-1418.3+512.47i	-1402.8+518.68i
18.	-1574.5-388.74i	-1446.7-498.86i	-1418.3-512.47i	-1402.8-518.68i
19.	-300.97+682.69i	-80.819+787.57i	-5.9768+793.29i	41.537+791.22i
20.	-300.97-682.69i	-80.819-787.57i	-5.9768-793.29i	41.537-791.22i
21.	-283.59+544.2i	-119.94+581.57i	-69.924+579.82i	-39.226+575.59i
22.	-283.59-544.2i	-119.94-581.57i	-69.924-579.82i	-39.226-575.59i
23.	-9.862+0i	-4.9564+0i	-3.4283+0i	-2.4728+0i
24.	-85.958+291.52i	-49.233+294.93i	-39.381+299.24i	-33.661+302.66i
25.	-85.958-291.52i	-49.233-294.93i	-39.381-299.24i	-33.661-302.66i

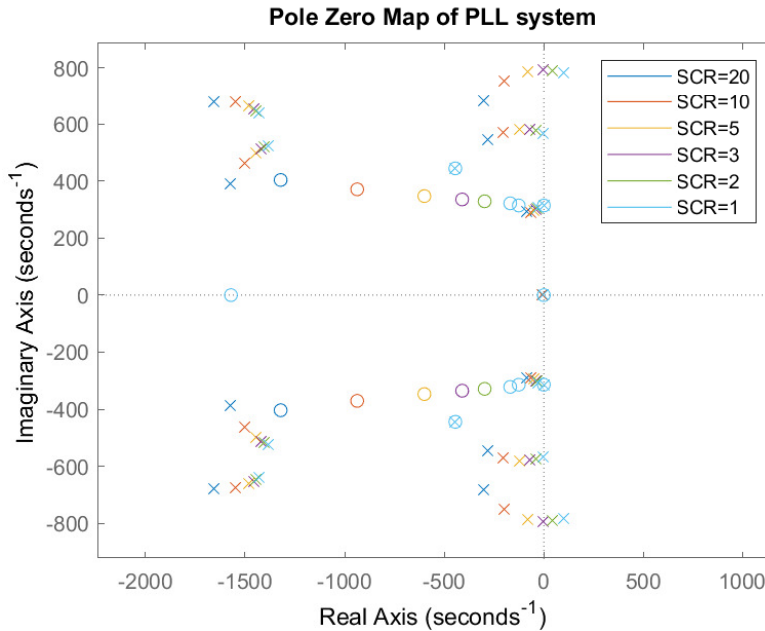
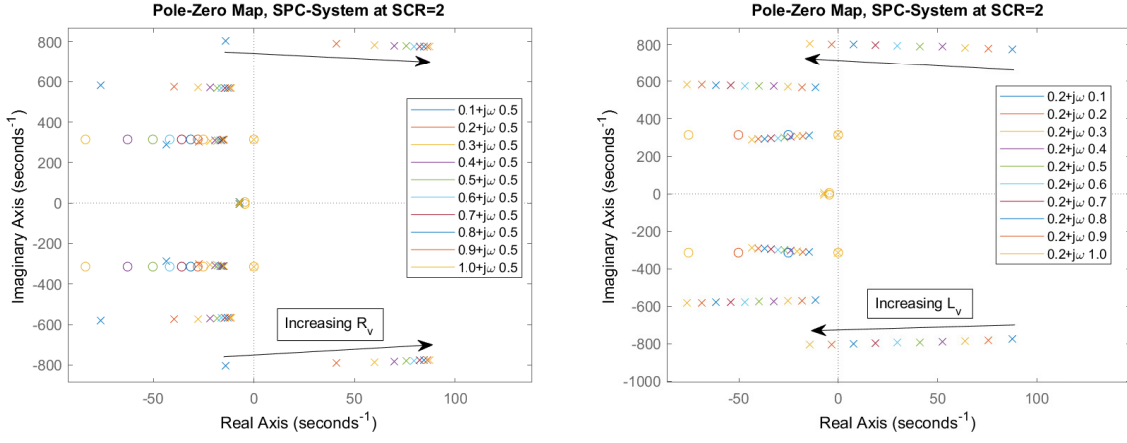


Figure 5.12: Pole-zero plot for the poles closes to the origin presented in Table 5.8.

Table 5.8 elucidates that the same poles as in the SPC-case moves to the right halfplane for SCR=2. The location is also almost exactly the same. This would indicate that it is presumably not the SPC-synchronization itself that results in the system becoming unstable for a weak grid but rather some common part of the system. This is fortified by the participation factors previously presented. Pole 19 and 20 displayed participation to the network model, hence it is reasonable that these poles are heavily affected by the change in grid strength.

However, it proves possible to counteract this introduced instability at low grid strengths by changing the value of the virtual admittance structure. In Figure 5.13 the pole locations for different settings of the virtual resistance and inductance is presented.



(a) Change of pole location with varying resistance. (b) Change of pole location with varying inductance.

Figure 5.13: Pole-zero plot for the poles closest to the imaginary axis for the SPC-system at SCR=2.

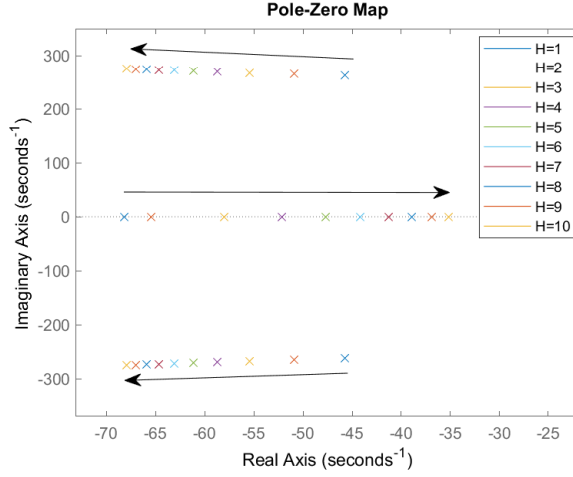
Figure 5.13 illustrates that the system goes unstable for $L_v < 0.9$ assuming that $R_v = 0.2$. By instead varying the virtual resistance and maintaining the virtual inductance at $L_v = 0.5$ it can be observed that the system is unstable for $R_v > 0.1$. However, it proves to be possible to counteract the introduced instability at low grid strengths by changing the value of the virtual admittance structure. Since the virtual admittance is part of the control system its parameters can also be varied during operation. This implies that it is possible to change the behavior of the control in order to ensure good performance also in situations with poor grid strength.

5.2.5 SPC Power Loop Parameters

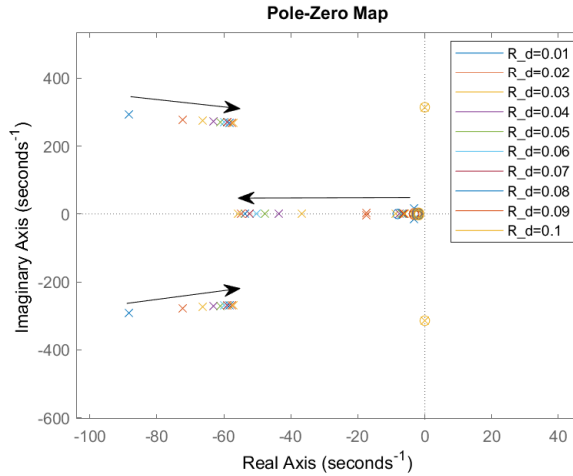
This section seeks to further investigate the influence of the inertia constant, H , the $P - f$ droop slope, R_d , and the damping factor, ξ , on the pole locations and will relate to the results presented in section 5.1.1. In Figure 5.14 a pole-zero plot is presented where the SPC-power loop parameters are varied.

The analysis using participation factors concluded that pole 23 and 24 were connected to the SPC-synchronization. By looking at how these poles change, a good understanding of how the different loop parameters influence the synchronization can be obtained. In Figure 5.14 (a), one can notice that pole 24 (placed on the real axis) moves to the right for increasing H . The same holds for pole 23 (not visible in the graph). This indicates that larger inertia constants tend to slow down the response. Interestingly it can also be noted that other poles show the opposite behavior, moving to the left for increasing H . Also a reduced damping behavior can be noticed. This is true for pole 25 and 26, that showed participation with the network model. It is therefore not obvious how the overall system response is affected by a change in inertia constants, but since the SPC-poles are placed closer to the origin it is likely that they will be more dominating in determining the system characteristics than poles placed further away.

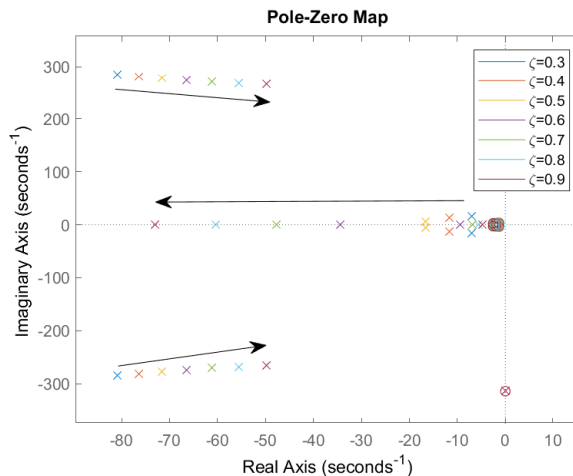
The change of droop slope, illustrated in Figure 5.14 (b), shows the same conflicting behavior in terms of response time. The SPC-related poles move to the left for an increased slope while other poles move to the right. However the system damping is enhanced for larger droop slopes, this pattern is visible for several pole locations. Figure (c) of 5.14 illustrates the effect of the damping factor. It can be concluded that larger damping factors gives better damping performance. For the SPC-loop this also improves the system response time.



(a) Change in pole location for different inertia constants, H .



(b) Pole locations with different droop slopes, R_d .



(c) Influence of damping factor, ξ , on pole locations.

Figure 5.14: Investigation on how the different SPC-loop parameters affect pole locations.

Chapter 6

Discussion

Chapter 3 introduced the concepts of grid-following, grid-forming and partial grid-forming control and presented three suitable grid-forming control methods. These control methods are discussed in Section 3.2.4. In Chapter 5 the analysis was focused on the SPC-method that were evaluated in terms of frequency and voltage behavior as well as converter stability, the implication of these results will be further discussed in this section.

Frequency and Voltage Behavior

Focusing on the frequency behavior, it can be noted from Figure 5.2 that the SPC-method synchronizes with the grid based on active power transfer. This implies that active power is exchanged with the grid in such a way that the synchronization is preserved. Hence, the method displays a similar behavior to a synchronous machine. This is further supported by the active power response due to a grid frequency change. The SPC-control sends out power to compensate for a decrease in frequency and similarly consumes power in order to compensate for an increase in frequency. In Figure 5.2 it can be observed that this change in the direction of power transfer is controlled by the current. By studying the power responses one can also note that power is transferred at a higher level for a transient period and than reaches a steady state value. This resembles the behavior of a synchronous machine where power can be absorbed from the rotating mass and transferred to the grid. This transient period implies that the SPC-control method incorporates the ability to provide frequency response services to the grid and provide so called synthetic inertia. It can be noted from the response in Figure 5.2 that the SPC-method do not only act on the ROCOF, but also actively tries to restore the frequency on the grid to the specified reference value by transferring power to/from the grid. The SPC-method also has an advantage compared to the other grid-forming methods introduced in Chapter 3 since it has the ability to change the characteristics of the response by adjusting the power-loop parameters, as seen in Figure 5.3. The power-loop parameters, H , R_d and ξ can be chosen without the constraints that physical generators are limited by. This provides the ability to adjust the power response to the desired behavior, provided that the converter stability is maintained. For example, the inertia constant, H , can be altered in order to change the behavior of the transient period of the power response and therefore governs the amount of synthetic inertia in the system. A change in H will influence the K_p , K_I and K_g parameters and therefore alter the performance of the SPC power synchronization loop.

Instead looking into the voltage behavior, it is notable that the SPC-method do not implement an ordinary voltage regulator but rather a virtual admittance structure. This practically means that the current reference is obtained by calculating a voltage drop over the admittance. By studying Figure 5.5 it can be noted that the virtual admittance structure provides a voltage forming behavior to the SPC-method since it is able to regain to the specified voltage level after a disturbance. The virtual admittance structure also introduces the possibility to ensure a high X/R-ratio so that the assumptions for (3.11) is valid. Figure 5.5 also illustrates that one should be careful to classify all PLL-based systems as grid following. The PLL-system implemented with a voltage controller shows a similar voltage behavior to the SPC-method and should be regarded as a partially grid-forming system.

Pole Locations

In Table A.1 it can be observed that the system poles are located in the left half-plane and thus the system is stable. However, a pole pair is placed at $0 \pm 314.16i$ for both the PLL and SPC-system. A pole placed on the imaginary axis would indicate that the system is only marginally stable. The investigation however concluded that this pole originates from the $\alpha\beta/dq$ -transformation and is thus not related to the control method itself. In Table A.1 several matching poles and zeros can be noted. These poles are considered to be canceled by their equivalent zeros and is therefore not further analyzed. As stated in Chapter 2, the concept of pole-zero cancellation is not to be considered as a precise tool to be used in regulator design but rather as a convenient concept. This is how the concept of pole-zero cancellation is applied in this study. Even though there is a small mismatch between the pole and zero one can assume that the influence of the pole in the overall response is small and it is motivated to not further analyze that pole. Several of these cancelled poles could also be traced to the different filters implemented in the system.

By comparing the pole locations of the SPC- and PLL-systems in Table 5.4 it can be observed that the systems have different pole locations, but the stability of the converter is preserved when the synchronization is restructured from a grid-following to a grid-forming control. The grid-following system (denoted GFL-PLL in Table 5.4) shows different pole locations compared to the PLL and SPC-system. This is reasonable since the GFL-PLL does not incorporate any voltage control and hence the system behavior is different, as seen in Figure 5.5. In Table 5.4 it is presented that the SPC-system has a slower response than the PLL-system. This is however related to the parameters of the power-synchronization loop and in Table 5.5 the SPC-system have been adjusted in order to match the PLL pole locations. It can be seen that it is possible to change the SPC-parameters in such a way that the pole locations are close to match. This would indicate that the two ways of performing the synchronization can behave in a similar way but if they in fact perform the same control action needs further investigation. The PLL regulates v_q voltage, and hence the reactive power, to zero and is therefore also based on power transfer in order to establish synchronism. It could also be questioned whether it is the virtual admittance structure, implemented in both the SPC and GFM-PLL system, that makes it possible to match the SPC and PLL poles since it introduces a VSC behavior.

Section 5.2.4 describes the grid strength impact on the pole locations. In Table 5.7 and 5.8 it can be noted that both the SPC and PLL-system becomes unstable in a weak grid situation. It is pole number 19 and 20 that introduces the instability. The participation factors imply that these poles are related to the network model of the system. Since the grid strength is reduced, the network model (in the state space model) will consequently be less stable, and as it turns out, in fact unstable. However, it is possible to counteract this instability by adjusting the values of the virtual admittance structure. Therefore, the virtual admittance structure introduces the ability to adapt the converter behavior according to the grid strength. This is an advantage compared to the other grid forming control methods introduced in Chapter 3, since those methods don't offer the same flexibility in changing the voltage forming behavior. However, it is important to note that a weak grid in this investigation was obtained by reducing the SCR of the network. The weak grid therefore has poor grid strength but still has high inertia. Further studies investigating low inertia is thus recommended.

Validity of Results and Modelling Errors

All modelling and simulation work are associated with errors and uncertainties. It is easy to interpret simulation results as an absolute fact when the results are presented. It is therefore of utmost importance to remember that a model is a mathematical description of a system that tries to capture a certain behavior. A model can never be a “true” or exact representation of a physical system, instead the model is developed with the purpose of solving a specific problem. In this thesis the purpose was to investigate the behavior that certain control methods display, rather than calculate explicit electrical quantities. With that said, the model must still be able to calculate electrical quantities, such as voltage and current, with precision in order to show the correct behavior. But the goal with the modelling work was not to be able to determine the converter current with an accuracy of 16 digits, for that implementation other models should be considered. The reader should therefore focus on assessing the behavior that the results imply rather than on the specific number itself.

Two models were created in this study, one continuous time model and one linearized model. In order to ensure that these two models describe the same system they were extensively validated against each

other, as presented in Chapter 4 and Appendix C. The fact that two models are produced describing the same system should ensure that the correct system behavior is captured in these models. The risk of modelling errors is reduced when the modelling is done twice and using two models also makes it possible to compare the two model responses. One could argue that it is possible that the same error could be reproduced in both models and the error would therefore not be observable by comparing the responses. It is however unlikely that this is true. The two models are fundamentally different since one is a continuous time simulation that is based on the Simulink environment and Simscape package while the other is a linearized model, based on state space representations. The two models therefore use two separate tools to describe the same system dynamics and therefore the risk of implementing the same modelling error is reduced.

As presented in section 4.3, the two models were validated against each other. It can be seen that the responses of the two models are much alike but some minor differences can be noted. As discussed above, it is important that the models display the same behavior and some discrepancies between the responses can be tolerated without further implications.

Tuning of PI-Controllers

The procedure of tuning the PI-controllers and control loops focused on obtaining a well performing system that is fast but still robust. However, the tuning work turned out to be much time consuming and had to be somewhat limited in order to not exceed the project time frame. Therefore, it is possible that the PI-gains can be further adjusted in order to obtain an even better performing system. Nevertheless, the presented results are based on a well performing system and the validity of the results will not be affected by and further tuning of the PI-gains since this increase in performance will manifest itself in both the grid-forming and grid-following system.

Suggestions for Further Studies

This thesis assumes that no restrictions is placed on the energy storage system connected to the VSC. It can be questioned whether this is a valid assumption to make. In physical applications it will of course not be possible to perform grid-forming control with an infinite energy storage, but the scope of this thesis is to identify if it is possible or not to provide frequency/power support services to the grid. Putting restrictions on the energy storage will not influence if a grid-forming VSC can or cannot provide these services but would rather influence the timescale of the response. It is however encouraged for further studies to incorporate a model of the energy storage system in order to be able to further analyze the ability to provide fast frequency response services. The result of this thesis indicate that there are similarities between a grid-forming and a grid-following synchronization. It is recommended that the investigation on the similarities between these two ways of synchronizing to the grid is continued. It is also recommended for future studies to further analyze the two control methods that were introduced in Chapter 3, but not further analyzed, to gain insights in their grid-forming behavior.

This study has focused on identifying voltage and frequency behavior and investigating the converter stability. However, there are several other aspects that needs to be considered before grid-forming control methods can be applied on real-life utility installations e.g. the fault ride through capability and the inrush current. A study investigating the interaction between several grid-forming converters in an area is also recommended. As with all components in the power system, it is of utmost importance that their behavior and properties are well known. Underperforming or faulty components can result in critical power system situations and possibly cause blackouts with massive impact on the modern society.

Chapter 7

Conclusion

This thesis presents three suitable grid-forming control methods for VSCs and further analyzed one of these methods, known as synchronous power control (SPC). The overall concept of grid-forming control is for the converter to behave similarly to a synchronous machine and the control concept is therefore inspired by the swing equation dynamics. This results in that grid-forming control methods will operate around a specified operating point and adjust the outputs accordingly. A grid-following control method instead adjusts the output to match measured grid quantities.

The investigation shows that the SPC-method has the ability to provide frequency response services and so called “synthetic inertia” to the grid. The stability of the converter is not affected in a major way and stability is preserved when the control is restructured from grid-following to grid-forming. By adjusting some control parameters, stability can also be ensured in situations with poor grid strength.

Bibliography

- [1] G. Denis, T. Prevost, M. Debry, F. Xavier, X. Guillaud, and A. Menze, “The migrate project: The challenges of operating a transmission grid with only inverter-based generation. a grid-forming control improvement with transient current-limiting control”, *IET Renewable Power Generation*, vol. 12, no. 5, pp. 523–529, 2018, ISSN: 1752-1424. DOI: 10.1049/iet-rpg.2017.0369.
- [2] U. Markovic, O. Stanojev, P. Aristidou, and G. Hug, “Partial grid forming concept for 100% inverter-based transmission systems”, en, in *2018 IEEE Power Energy Society General Meeting (PESGM)*, Power Energy Society General Meeting (PESGM); Conference Location: Portland, OR, USA; Conference Date: August 5-10, 2018, Piscataway, NJ: IEEE, 2018, p. 8586114, ISBN: 978-1-5386-7703-2. DOI: 10.3929/ethz-b-000310719.
- [3] B. Kroposki, B. Johnson, Y. Zhang, V. Gevorgian, P. Denholm, B. Hodge, and B. Hannegan, “Achieving a 100% renewable grid: Operating electric power systems with extremely high levels of variable renewable energy”, *IEEE Power and Energy Magazine*, vol. 15, no. 2, pp. 61–73, 2017, ISSN: 1558-4216. DOI: 10.1109/MPE.2016.2637122.
- [4] P. 2017/18:22, *Regeringens proposition 2017/18:228 - energipolitikens inriktning*, <https://www.regeringen.se/497262/contentassets/5fe7ecdee2b440eb81348fc722324c91/energipolitikens-inritkning-prop.-201718228>, Accessed: 2020-02-10.
- [5] J. Rocabert, A. Luna, F. Blaabjerg, and P. Rodríguez, “Control of power converters in ac microgrids”, *IEEE Transactions on Power Electronics*, vol. 27, no. 11, pp. 4734–4749, Nov. 2012, ISSN: 1941-0107. DOI: 10.1109/TPEL.2012.2199334.
- [6] R. Lasseter, Z. Chen, and D. Pattabiraman, “Grid-forming inverters: A critical asset for the power grid”, *IEEE Journal of Emerging and Selected Topics in Power Electronics*, pp. 1–1, 2019, ISSN: 2168-6785. DOI: 10.1109/JESTPE.2019.2959271.
- [7] R. Adapa, M. Baker, L. Bohmann, K. Clark, K. Habashi, L. Gyugyi, J. Lemay, A. Mehraban, A. Myers, J. Reeve, F. Sener, D. Torgerson, and R. Wood, “Proposed terms and definitions for flexible ac transmission system (facts)”, *IEEE Transactions on Power Delivery*, vol. 12, no. 4, pp. 1848–1853, Oct. 1997, ISSN: 1937-4208. DOI: 10.1109/61.634216.
- [8] P. Schavemaker and L. Sluis, *Electrical Power System Essentials*, 2nd edition. Wiley, Jul. 2017, ISBN: 978-1-118-80347-9.
- [9] L. L. Grigsby, *Power System Stability and Control*, 3rd ed. CRC Press LLC, 2012, ISBN: 9781439883204.
- [10] T. Navpreet, M. Tarun, B. Amit, J. Kotturu, S. Bhupinder, B. Anant, and S. Gurangel, “Voltage source converters as the building block of hvdc and facts technology in power transmission system: A simulation based approach”, *Advances in Applied Science Research*, vol. 3, 2012.
- [11] M. Priya, P. Ponambalam, and K. Muralikumar, “Modular-multilevel converter topologies and applications – a review”, *IET Power Electronics*, vol. 12, no. 2, pp. 170–183, 2019.
- [12] F. Martinez-Rodrigo, D. Ramirez, A. Rey-Boué, S. Depablo, and L. Lucas, “Modular multilevel converters: Control and applications”, *Energies*, vol. 10, p. 1709, Oct. 2017. DOI: 10.3390/en10111709.
- [13] B. Lennartsson, *Reglerteknikens grunder*, 4th ed. Studentlitteratur, 2002, ISBN: 9789144024165.
- [14] W. S. Levine, *The Control Handbook*. CRC Press, 1996, ISBN: 9780849385704.
- [15] P. Kundur, N. Balu, and M. Lauby, *Power system stability and control*. McGraw-Hill New York, 1994, vol. 23.
- [16] A. Yazdani and R. Iravani, in *Voltage-Sourced Converters in Power Systems: Modeling, Control, and Applications*. IEEE, 2010, pp. i–xix, ISBN: 9780470551561. DOI: 10.1002/9780470551578.

- [17] W. Zhang, D. Remon, and P. Rodriguez, “Frequency support characteristics of grid-interactive power converters based on the synchronous power controller”, *IET Renewable Power Generation*, vol. 11, no. 4, pp. 470–479, 2017, ISSN: 1752-1424. DOI: 10.1049/iet-rpg.2016.0557.
- [18] L. Zhang, L. Harnefors, and H. Nee, “Power-synchronization control of grid-connected voltage-source converters”, *IEEE Transactions on Power Systems*, vol. 25, no. 2, pp. 809–820, May 2010, ISSN: 1558-0679. DOI: 10.1109/TPWRS.2009.2032231.
- [19] A. Engler and N. Soultanis, “Droop control in lv-grids”, 6 pp.–6, Nov. 2005. DOI: 10.1109/FPS.2005.204224.
- [20] A. Tuladhar, H. Jin, T. Unger, and K. Mauch, “Parallel operation of single phase inverter modules with no control interconnections”, vol. 1, 94–100 vol.1, Feb. 1997. DOI: 10.1109/APEC.1997.581439.
- [21] Y. A. I. Mohamed and E. F. El-Saadany, “Adaptive decentralized droop controller to preserve power sharing stability of paralleled inverters in distributed generation microgrids”, *IEEE Transactions on Power Electronics*, vol. 23, no. 6, pp. 2806–2816, Nov. 2008, ISSN: 1941-0107. DOI: 10.1109/TPEL.2008.2005100.
- [22] J. M. Guerrero, Luis Garcia de Vicuna, J. Matas, M. Castilla, and J. Miret, “Output impedance design of parallel-connected ups inverters with wireless load-sharing control”, *IEEE Transactions on Industrial Electronics*, vol. 52, no. 4, pp. 1126–1135, Aug. 2005, ISSN: 1557-9948. DOI: 10.1109/TIE.2005.851634.
- [23] J. M. Guerrero, J. Matas, L. G. de Vicuna, N. Berbel, and J. Sosa, “Wireless-control strategy for parallel operation of distributed generation inverters”, vol. 2, 845–850 vol. 2, Jun. 2005, ISSN: 2163-5145. DOI: 10.1109/ISIE.2005.1529025.
- [24] S. J. Chiang, C. Y. Yen, and K. T. Chang, “A multimodule parallelable series-connected pwm voltage regulator”, *IEEE Transactions on Industrial Electronics*, vol. 48, no. 3, pp. 506–516, Jun. 2001, ISSN: 1557-9948. DOI: 10.1109/41.925577.
- [25] A. Engler, “Control of parallel operating battery inverters”, Jan. 2000.
- [26] J. Meng, Y. Wang, C. Fu, and H. Wang, “Adaptive virtual inertia control of distributed generator for dynamic frequency support in microgrid”, pp. 1–5, Sep. 2016. DOI: 10.1109/ECCE.2016.7854825.
- [27] J. M. Cajigal-Núñez, P. Winter, and H. Wrede, “Modern control method of mmc statcom for future power grids”, in *2019 21st European Conference on Power Electronics and Applications (EPE '19 ECCE Europe)*, 2019, P.1–P.6.
- [28] Q. Zhong and G. Weiss, “Synchronverters: Inverters that mimic synchronous generators”, *IEEE Transactions on Industrial Electronics*, vol. 58, no. 4, pp. 1259–1267, Apr. 2011, ISSN: 1557-9948. DOI: 10.1109/TIE.2010.2048839.
- [29] J.-S. Meng, S.-h. Chen, C.-H. Zhang, X. Chen, Q.-C. Zhong, Z.-p. Lv, and Q. Huang, “An improved synchronverter model and its dynamic behaviour comparison with synchronous generator”, Jan. 2013, pp. 4.13–4.13, ISBN: 978-1-84919-758-8.
- [30] J. Driesen and K. Visscher, “Virtual synchronous generators”, pp. 1–3, Jul. 2008, ISSN: 1932-5517. DOI: 10.1109/PES.2008.4596800.
- [31] H. Beck and R. Hesse, “Virtual synchronous machine”, pp. 1–6, Oct. 2007, ISSN: 2150-6655. DOI: 10.1109/EPQU.2007.4424220.
- [32] T. Jouini, C. Arghir, and F. Dörfler, “Grid-friendly matching of synchronous machines by tapping into the dc storage**this research is supported by eth funds and the snf assistant professor energy grant 160573.”, *IFAC-PapersOnLine*, vol. 49, no. 22, pp. 192–197, 2016, 6th IFAC Workshop on Distributed Estimation and Control in Networked Systems NECSYS 2016, ISSN: 2405-8963.
- [33] S. D’Arco and J. A. Suul, “Virtual synchronous machines — classification of implementations and analysis of equivalence to droop controllers for microgrids”, pp. 1–7, Jun. 2013. DOI: 10.1109/PTC.2013.6652456.
- [34] V. Natarajan and G. Weiss, “Synchronverters with better stability due to virtual inductors, virtual capacitors, and anti-windup”, *IEEE Transactions on Industrial Electronics*, vol. 64, no. 7, pp. 5994–6004, Jul. 2017, ISSN: 1557-9948. DOI: 10.1109/TIE.2017.2674611.
- [35] B. B. Johnson, M. Sinha, N. G. Ainsworth, F. Dörfler, and S. V. Dhople, “Synthesizing virtual oscillators to control islanded inverters”, *IEEE Transactions on Power Electronics*, vol. 31, no. 8, pp. 6002–6015, Aug. 2016, ISSN: 1941-0107. DOI: 10.1109/TPEL.2015.2497217.

Appendix A

Analysis of Pole Locations for Model Components

In this chapter the pole and zero locations of the GFM-PLL- and GFM-SPC-system is presented, as seen in Table A.1. Matching poles and zeros are marked in gray for the PLL-system and in blue for the SPC-system.

In Table A.1 it can be seen that there are no right-half-plane poles, indicating that the PLL and SPC systems are stable. There are also several poles that are canceled by equivalent zeros. It is worth investigating where the different poles originate from to get further insights on the system. An investigation of the poles of each system block will follow. The poles of each system component can then be compared with the poles displayed in Table A.1 to see if they are visible in the closed loop transfer function.

Low-Pass Filter

A low-pass filter is implemented to take system sampling delays into consideration. The filter transfer function is

$$H_{ZOH}(s) = \frac{1}{\frac{s}{\omega_c} + 1} \quad (\text{A.1})$$

where $\omega_c = 3000 \cdot \pi \cdot 2$ rad/s, hence

$$H_{ZOH}(s) = \frac{18850}{s + 18850}, \quad (\text{A.2})$$

giving a pole in $-18850 + 0i$. The pole can be observed in Table A.1. The low pass filter is used several times in the state space model, explaining the multiple poles in the closed-loop transfer function.

Low-pass filter on dq-voltage and current

The low-pass filter is implemented as

$$H_{LP}(s) = \frac{a^2}{s^2 + 2\sqrt{a}s + a^2} \quad (\text{A.3})$$

where $a = 2\omega_{grid}$, implying

$$H_{LP}(s) = \frac{3.948 \cdot 10^5}{s^2 + 888.6s + 3.948 \cdot 10^5}, \quad (\text{A.4})$$

resulting in a pole at $-444.3 \pm 444.3i$. Also this filter is observed in Table A.1 and since it is used for both dq-voltages and currents the pole is introduced four times in the closed loop transfer function.

Pole at $0 \pm 314.16i$

The pole located at $0 \pm 314.16i$ is concerning since a pole on the imaginary axis can indicate that the system is only marginally stable. One hypothesis is however that the dq-transformation introduces a pole at $0 \pm 314.16i$, since 314.16 is the grid frequency (50 Hz) in rad/s. To test the hypothesis a capacitor is implemented as a state space representation in the $\alpha\beta$ -frame. A capacitor has the transfer function

$$H(s) = \frac{1}{sC} \quad (\text{A.5})$$

Table A.1: Poles and zeros for the GFM-PLL and GFM-SPC systems. The table can be used to identify matching poles and zeros, marked in gray for the PLL case and blue for the SPC-case.

Nr	GFM-PLL Poles	GFM-PLL Zeros	GFM-SPC Poles	GFM-SPC Zeros
1.	-4.7703+2.0276e+08i	-1e+18+0i	-4.7703+2.0276e+08i	-444.29+444.29i
2.	-4.7703-2.0276e+08i	-1e+18+0i	-4.7703-2.0276e+08i	-444.29-444.29i
3.	-4.7703+2.0276e+08i	-12.179+2.0152e+07i	-4.7703+2.0276e+08i	-1e+18+0i
4.	-4.7703-2.0276e+08i	-12.179-2.0152e+07i	-4.7703-2.0276e+08i	-1e+18+0i
5.	-12.218+1.4309e+07i	-12.179+2.0151e+07i	-12.218+1.4309e+07i	-12.179+2.0152e+07i
6.	-12.218-1.4309e+07i	-12.179-2.0151e+07i	-12.218-1.4309e+07i	-12.179-2.0152e+07i
7.	-12.218+1.4308e+07i	-22665+5491.3i	-12.218+1.4308e+07i	-12.18+2.0151e+07i
8.	-12.218-1.4308e+07i	-22665-5491.3i	-12.218-1.4308e+07i	-12.18-2.0151e+07i
9.	-22630+5535.5i	-22631+5535.3i	-22631+5534.9i	-22665+5491.9i
10.	-22630-5535.5i	-22631-5535.3i	-22631-5534.9i	-22665-5491.9i
11.	-22665+5491.2i	-9959.4+133.49i	-22665+5491.7i	-22631+5534.8i
12.	-22665-5491.2i	-9959.4-133.49i	-22665-5491.7i	-22631-5534.8i
13.	-9961.1+135.55i	-1321.3+403.64i	-9960.9+132.29i	-18850+0i
14.	-9961.1-135.55i	-1321.3-403.64i	-9960.9-132.29i	-9959.2+130.23i
15.	-1654.7+678.74i	-0.0017179+314.16i	-1654+676.48i	-9959.2-130.23i
16.	-1654.7-678.74i	-0.0017179-314.16i	-1654-676.48i	-18850+0i
17.	-1574.5+388.74i	-125.66+314.16i	-1576+389.09i	-18850+0i
18.	-1574.5-388.74i	-125.66-314.16i	-1576-389.09i	-1319.4+394.56i
19.	-300.97+682.69i	3.3293e-12+0i	-299.15+693.97i	-1319.4-394.56i
20.	-300.97-682.69i	-1570.8+0i	-299.15-693.97i	-1570.8+0i
21.	-283.59+544.2i	-18850+0i	-287.53+540.99i	-125.66+314.16i
22.	-283.59-544.2i	-18850+0i	-287.53-540.99i	-125.66-314.16i
23.	-9.862+0i	-18850+0i	-6.9082+0i	-0.0017176+314.16i
24.	-85.958+291.52i	-1570.8+0i	-48.903+0i	-0.0017176-314.16i
25.	-85.958-291.52i	-444.29+444.29i	-61.207+271i	-3.0008+3.9925i
26.	-0.0016397+314.16i	-444.29-444.29i	-61.207-271i	-3.0008-3.9925i
27.	-0.0016397-314.16i	-444.29+444.29i	-0.0016551+314.16i	-1570.8+0i
28.	-444.29+444.29i	-444.29-444.29i	-0.0016551-314.16i	-444.29+444.29i
29.	-444.29-444.29i	-444.29+444.29i	-444.29+444.29i	-444.29-444.29i
30.	-444.29+444.29i	-444.29-444.29i	-444.29-444.29i	-444.29+444.29i
31.	-444.29-444.29i	-444.29+444.29i	-444.29+444.29i	-444.29-444.29i
32.	-18850+0i	-444.29-444.29i	-444.29-444.29i	-18850+0i
33.	-18850+0i	-18850+0i	-18850+3.8781e-05i	-444.29+444.29i
34.	-18850+0i	-	-18850-3.8781e-05i	-444.29-444.29i
35.	-18850+0i	-	-18850+0i	-18850+0i
36.	-18850+0i	-	-18850+0i	-18850+0i
37.	-18850+0i	-	-18850+9.0631e-11i	-
38.	-	-	-18850-9.0631e-11i	-
39.	-	-	-18850+3.4989e-11i	-
40.	-	-	-18850-3.4989e-11i	-

where C is the capacitance. The state space model is obtained with the methodology described in Chapter 4. From the transfer function it can be noted that the pole is located at 0. The $\alpha\beta$ -model is then transformed into dq-space by applying the rotation matrix. Figure A.1 shows the pole-zero plot of the capacitance model in $\alpha\beta$ and dq-space.

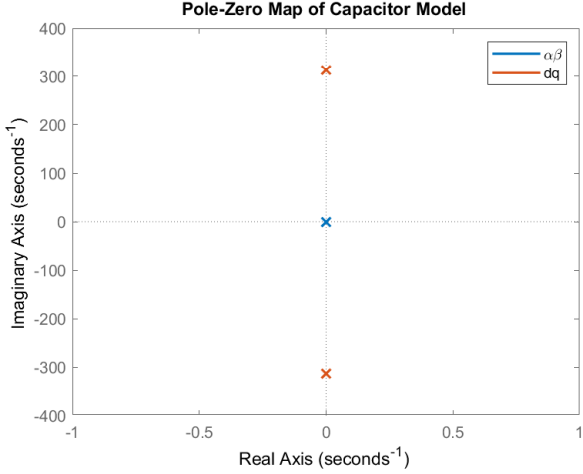


Figure A.1: Pole-zero plot of the capacitor model in $\alpha\beta$ and dq-space.

From Figure A.1 it can be noted that the pole is located at 0 in the $\alpha\beta$ -frame but is moved to $0 \pm 314.16i$ in dq-space. It can therefore be concluded that the pole in the closed loop transfer function, displayed in Table A.1 originates from the dq-transformation and is not specific to the PLL- or SPC-system. The pole is also canceled by a corresponding zero and will likely not influence the converter stability.

Feed Forward Filter

The feed forward filter is defined as

$$H(s) = \frac{a_1}{s + a_1} \quad (\text{A.6})$$

where $a_1 = 5 \cdot \omega = 5 \cdot 50 \cdot 2\pi$ rad/s, that implies

$$H(s) = \frac{1571}{s + 1571}. \quad (\text{A.7})$$

The feed forward filter thus introduce a pole at -1571 . In the closed loop transfer function a pole at $-1576 \pm 389i$ can be observed, but no exact match with the feed forward filter pole is noted.

Virtual Admittance

The pole polynomial of the virtual admittance transfer function is

$$r(s) = s^2 + 251.3s + 1.145 \cdot 10^5. \quad (\text{A.8})$$

Solving for $r(s) = 0$ gives the pole location $-125.6 \pm 314.16i$. No such pole can be observed in Table A.1.

Converter Reactor

The converter reactor has the following pole polynomial,

$$r(s) = s^2 + 62.83s + 9.97 \cdot 10^4. \quad (\text{A.9})$$

Solving for the poles, gives the pole locations at $-31.42 \pm 314.16i$. By studying Table A.1 it can be concluded that no such pole is present in the closed loop transfer function.

Primary & Secondary Filters

The d- and q-component of the transfer function is

$$\begin{aligned} H_1(s) &= \frac{4.34 \cdot 10^{10}s}{s^2 + 9.87 \cdot 10^4} \\ H_2(s) &= \frac{-1.36 \cdot 10^{13}}{s^2 + 9.87 \cdot 10^4}, \end{aligned} \quad (\text{A.10})$$

which gives poles at $0 \pm 314.16i$. One such pole pair is observed in Table A.1, however it has already been concluded that it originates from the dq-transformation.

Transformer

The transformer state space model has four inputs and four transfer functions for every input. However, the pole polynomial is the same for these transfer functions,

$$r(s) = s^4 + 18.85s^3 + 1.975 \cdot 10^5 s^2 + 1.86 \cdot 10^6 s + 9.75 \cdot 10^9 \quad (\text{A.11})$$

that gives the poles $-9.42 \pm 314.16i$ and $0 \pm 314.16i$. Unfortunately, these poles are not observed in Table A.1.

Network Model

The pole polynomial describing the network model is,

$$r(s) = s^2 + 41.89s + 9.91 \cdot 10^4. \quad (\text{A.12})$$

By solving for the poles, $-20.9 \pm 314.16i$ is obtained, however no such poles are noted in Table A.1.

PLL-Block

The PLL-transfer function is

$$H(s) = K_p + \frac{K_i}{s} = \frac{0.0028s + 14.14}{s} \quad (\text{A.13})$$

and therefore has a pole at 0.

SPC-Block

The SPC-block transfer function is implemented as

$$H(s) = \frac{K_p s + K_i}{s + K_g} \cdot \frac{1}{s} = \frac{K_p s + K_i}{s^2 + K_g s}, \quad (\text{A.14})$$

with values inserted, the transfer function is

$$H(s) = \frac{5.074s + 31.42}{s^2 + 2s} \quad (\text{A.15})$$

and will therefore introduce a pole in 0 and -2. No such poles are visible in Table A.1.

Summary and Conclusion

In this section it has been observed that some of the filter poles can be directly observed in the closed loop transfer function. But it can also be noted that several poles of the different model components are not directly reproduced in the closed loop transfer function of the system model. This indicates that there are some interaction that shifts the pole locations for the majority of the poles in the closed-loop transfer function. The poles that needs further investigation are presented in Table 5.1.

Appendix B

Other Grid Forming Control Methods

Two other grid forming control methods that are not investigated in detail in this thesis are shortly presented in the following paragraphs.

Virtual Synchronous Generator

Virtual synchronous generators (VSG), also known as “synchronverters”, originates from the idea of operating an inverter to mimic a synchronous generator. Droop, PSC and SPC also have the purpose of operating similarly to a synchronous machine but the VSG concept takes the implementation one step further. With this implementation all the benefits of the synchronous generator are incorporated in the design, but so are also the downsides. However, since this is a power electronic-based system there are no physical limits to how the generator parameters can be chosen, making it possible to choose parameters that would be impossible in real life and also to change parameters during operation [28].

There are a large variety in the concept of VSGs where some concepts are much alike to the SPC-method while others, such as the synchronverter concept, models both the rotor and stator dynamics on a higher level. The complexity of these models vary from second to seventh order models where a third order model is widely used as a compromise between complexity and accuracy [29]. The interested reader is referred to [26], [30]–[34] for an in-depth description of the different VSG-concepts.

Virtual Oscillator

Compared to other control methods previously introduced that all utilizes dq- or $\alpha\beta$ -transformed quantities in the control loops, the virtual oscillator control is based on instantaneous time signals. This results in a quite different control methodology compared to the methods described earlier. The controller can be implemented as a Van der Pol oscillator and hence, an oscillating voltage waveform can be produced and sent to the PWM-generator according to the desired voltage amplitude and frequency. The process of generating these voltage waveforms is however associated with solving non-linear differential equations. It has been proven that the virtual oscillator can be tuned in order to give a similar response as a VSC with droop control would, read more about this in [35].

Appendix C

Continued Model Validation

In this chapter the results regarding system validation of some system components that can be validated will be presented. In the following figures the simulink model response will be presented in blue and the state space model response in orange.

Virtual Admittance

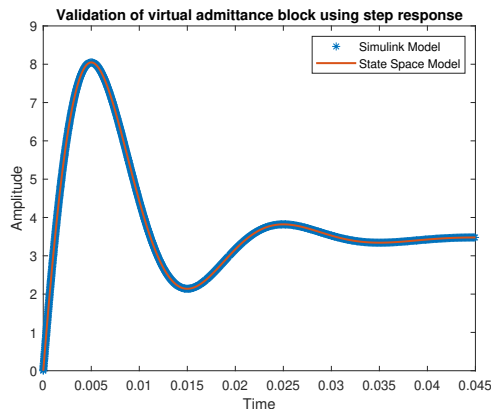


Figure C.1: Validation of the virtual admittance block.

Filter on dq-Voltage

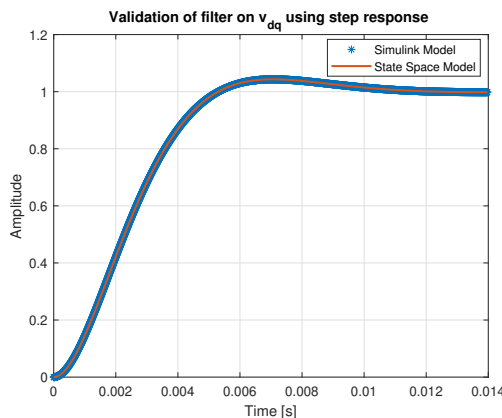


Figure C.2: Validation of the filter model that is applied on the v_{dq} voltage.

Current Controller

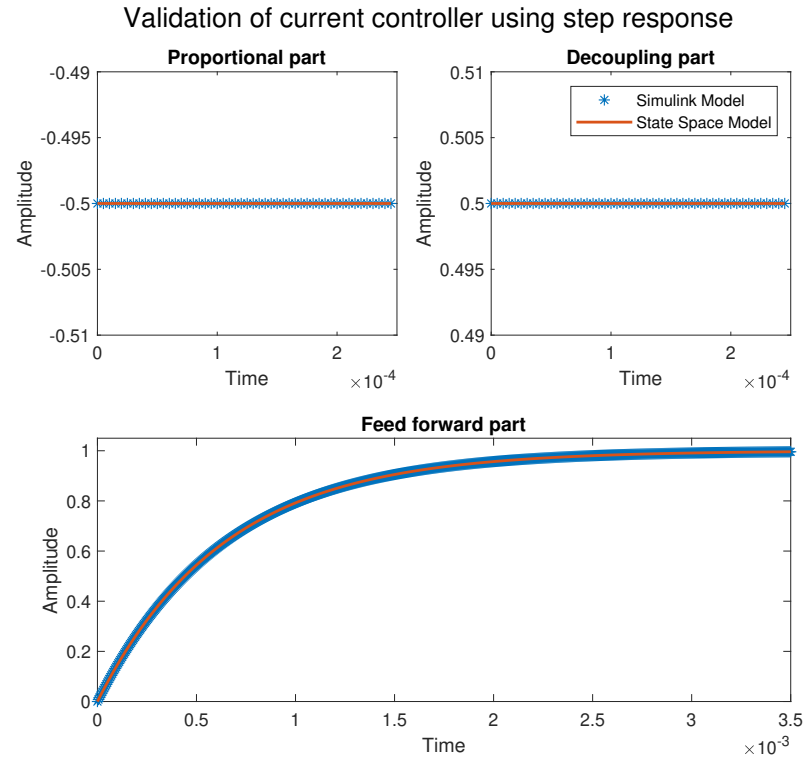


Figure C.3: Validation of current controller.

Filter on Feed Forward Term

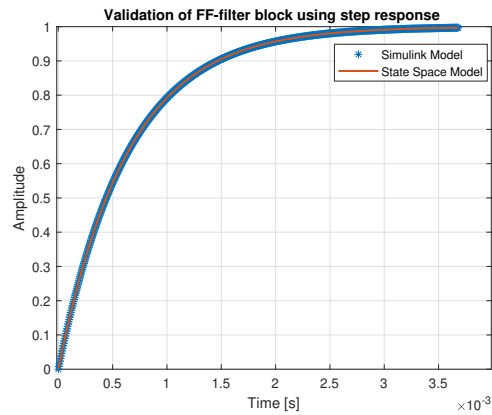


Figure C.4: Validation of filter on the feed forward term